Eur. Phys. J. C (2012) 72:1863
DOI 10.1140/epjc/s10052-012-1863-y

THE EUROPEAN PHYSICAL JOURNAL C

Regular Article - Theoretical Physics

Flavour and collider interplay for SUSY at LHC7

L. Calibbi[1,a], **R.N. Hodgkinson**[2,b], **J. Jones Pérez**[3,c], **A. Masiero**[4,5,d], **O. Vives**[2,e]

[1]Max-Planck-Institut für Physik (Werner-Heisenberg-Institut), Föhringer Ring 6, 80805 München, Germany
[2]Departament de Física Teòrica and IFIC, Universtat de València-CSIC, 46100 Burjassot, Spain
[3]INFN, Laboratori Nazionali di Frascati, Via E. Fermi 40, 00044 Frascati, Italy
[4]Dipartimento di Fisica, Università di Padova, via F. Marzolo 8, 35131 Padova, Italy
[5]INFN, Sezione di Padova, via F. Marzolo 8, 35131 Padova, Italy

Received: 9 December 2011 / Published online: 4 February 2012

Abstract The current 7 TeV run of the LHC experiment shall be able to probe gluino and squark masses up to values larger than 1 TeV. Assuming that hints for SUSY are found in the jets plus missing energy channel by the end of a 5 fb^{-1} run, we explore the flavour constraints on three models with a CMSSM-like spectrum: the CMSSM itself, a see-saw extension of the CMSSM, and Flavoured CMSSM. In particular, we focus on decays that might have been measured by the time the run is concluded, such as $B_s \to \mu\mu$ and $\mu \to e\gamma$. We also analyse constraints imposed by neutral meson bounds and electric dipole moments. The interplay between collider and flavour experiments is explored through the use of three benchmark scenarios, finding the flavour feedback useful in order to determine the model parameters and to test the consistency of the different models.

1 Introduction

The current run of the LHC, operating at $\sqrt{s} = 7$ TeV (LHC7 from now on), has been very successful and new results with significant improvements on our previous knowledge of the electroweak symmetry breaking (EWSB) energy region have been presented in the summer conferences and published afterwards. Although no Higgs or new physics (NP) signals have been found so far, LHC experiments have started to provide stringent test to the relevant extensions of the Standard Model (SM), in particular, to low-energy supersymmetry (SUSY). The most recent analyses based on $\sim$1 fb^{-1} of integrated luminosity already exclude squarks and gluinos, if close in mass, up to $\sim$1 TeV [1, 2]. Even though the relevant SUSY parameter space has not been fully explored yet, it is well known that naturalness arguments point towards a quite light spectrum of the SUSY particles.[1] Therefore, if SUSY is indeed realised at low energies as a theory related to the EWSB, we can expect some SUSY partners to lie in the reach of LHC7. This assumption is the starting point of the present work.

The Minimal Supersymmetric Standard Model (MSSM), understood as the minimal supersymmetric version of the SM with respect to the number of fields, can be considered the main goal of the early SUSY searches at the LHC. However, to explore the parameter space in a completely general MSSM is a formidable task given the huge number of unknown parameters (the number of "free" parameters in the MSSM being bigger than one hundred). This is the main reason why most of the analyses of SUSY phenomenology at collider experiments are made in the framework of the so-called Constrained Minimal Supersymmetric Standard Model (CMSSM), where all the soft SUSY breaking terms are assumed to be degenerate and only five parameters (beyond the already known SM parameters) are enough to define completely the model. In fact, this simple structure of the soft breaking terms can be found in some theoretical models, although complete flavour universality of the soft SUSY breaking is not generally true in most supergravity and string-inspired models.

On the other hand, the CMSSM can be hardly considered a satisfactory NP model, since it does not account neither for the peculiar hierarchy pattern we observe in the fermion masses and mixing nor for the generation of light neutrino

[a] e-mail: calibbi@mppmu.mpg.de
[b] e-mail: robert.hodgkinson@uv.es
[c] e-mail: joel.jones@lnf.infn.it
[d] e-mail: antonio.masiero@pd.infn.it
[e] e-mail: oscar.vives@uv.es

[1] After the first SUSY searches at the LHC, the fine-tuning price of the constrained MSSM is already at the percent level [3].

masses, which call for extension of the CMSSM. The existence and smallness of neutrino masses make it natural to extend the CMSSM in the direction of a supersymmetric seesaw mechanism [4–7], whilst the flavour puzzle of the Standard Model suggests a flavour model based on horizontal flavour symmetries [8]. It is, however, very unlikely that, even if SUSY is indeed discovered, the LHC alone can shed light on the flavour structure of the SUSY partners sector. Such extensions of the CMSSM (and to some extent the CMSSM itself) can be better probed and discriminated from other scenarios by means of the interplay between the LHC and the experiments dedicated to measure rare flavour changing or CP violating processes. Whilst we are witnessing a rich experimental activity with experiments already running like MEG and LHCb, with others under construction or development like SuperBelle, the Super Flavour Factory, $\mu \to e$ conversion experiments, on the theoretical side it is crucial to address the question of the complementarity of direct and indirect searches as a tool for discriminating among different SUSY models. For a detailed discussion of this problem we refer to [9]. Here we concentrate on the specific case of the present bounds and the expected near future sensitivity of LHC7.

In view of what was discussed above, in this work we mainly aim at answering the following questions: (i) what is the impact of the present limits on the SUSY spectrum provided by the LHC experiments on the capability of flavour experiments to observe deviations from the SM predictions? (ii) assuming that SUSY is indeed in the reach of the LHC7 searches, what are then the most promising channels probed at low-energy experiments where to look at in order to get more information about the fundamental SUSY parameters and discriminate among models?

In this paper, we try to address the above questions considering the interplay between direct SUSY searches at LHC7 and indirect searches in flavour and CP violation (CPV) experiments, within the CMSSM and some classes of phenomenologically motivated extensions of the CMSSM, which usually predict larger flavour and CPV effects than the CMSSM itself, namely SUSY seesaw and a Flavoured CMSSM, i.e. an extension of the CMSSM with non-trivial flavour structures in the sfermion sector. In particular, we are going to study the relevant flavour observables as predicted in the above mentioned models within the supersymmetric parameter space accessible at LHC7 up to 5 fb^{-1} of integrated luminosity, that is, the amount of data which should be collected and analysed between 2011 and 2012. Even though it is likely that by the end of 2012 both ATLAS and CMS might collect up to 10 fb^{-1}, we consider this conservative value since at the moment an increase of the centre of mass energy up 8 TeV during 2012 is still under consideration. Notice that we do not intend to do a fit of LHC data within these models, but to point out that all of these give similar collider signatures, and show that indirect experiments can help us differentiate between MSSM versions.

The rest of the paper is organised as follows: in the next section the current status and prospects of SUSY searches at LHC7 are briefly reviewed; the models we are going to study are discussed in Sect. 3; the numerical analysis is presented in Sect. 4; conclusions are drawn in Sect. 5.

2 SUSY searches at LHC7: current bounds and prospects

As a proton–proton collider, the search for SUSY at the LHC hinges upon the production of coloured squarks or gluinos through strong interactions. These heavy new particles are then expected to decay rapidly through a decay chain ending in one or more jets (by conservation of QCD colour), possibly leptons, and the lightest supersymmetric particle (LSP), which is stable under the assumption of R-parity conservation. To have escaped astrophysical and cosmological observations, the LSP must be a neutral particle and will hence escape the detector unseen. This leads to an apparent imbalance in the measured part of the final state, so that the characteristic signature of a SUSY process at the LHC is the "missing energy" (more accurately, missing momentum), $\not{E}_T$, associated with the unobserved LSP leaving the detector.

We have only limited knowledge of the partonic initial state in proton–proton collisions, in particular the boost of the partonic centre-of-mass frame relative to the lab-frame is not known and it is therefore impossible to reconstruct and measure the longitudinal momentum of any escaping neutral particle, such as the LSP. For this reason, LHC searches for SUSY look for an excess of events with two or more high transverse energy jets along with significant missing transverse energy.

In typical SUSY scenarios, the lightest coloured SUSY particle is usually either a gluino or a stop. The cross section for gluino pair-production at the LHC depends at leading order on only a single unknown parameter, the mass of the gluino itself. Indeed, the gluino production cross section at LHC7 is known to be large, $\sigma(pp \to \tilde{g}\tilde{g}) \gtrsim 100$ fb for gluinos of mass $m_{\tilde{g}} \lesssim 700$ GeV [10]. By contrast, the stop pair production cross section is around two orders of magnitude smaller for stop masses $m_{\tilde{t}} \sim m_{\tilde{g}}$ and so plays essentially no role in early LHC SUSY searches.

Although typically significantly heavier than the top- and bottom-squarks, the squarks of the first generation **do** play a role in the search strategy. The cross section for production of the up- and down-squarks is boosted by the presence of a t-channel gluino exchange diagram, with the valence quarks of the incoming protons in the initial state. The production

cross section for these first-generation squarks therefore depends on two parameters at leading order, the mass of both the exchanged gluino and that of the outgoing squarks themselves ($m_{\tilde{q}}$). The most stringent bounds on these parameters are already due to LHC results, which have overtaken the previous Tevatron and LEP bounds. Both ATLAS and CMS have published searches based on their initial 1 fb^{-1} data sets analysing the multi-jets plus missing energy and 0-lepton final state [1, 2]. The exclusion limits of both experiments are currently comparable. They set a mass limit of about 1 TeV for $m_{\tilde{g}} \simeq m_{\tilde{q}}$.

In the event of a discovery, of course, we can also expect to learn something more about the scale of SUSY. Inclusive searches in the 0-lepton channel look for events with two or more high-energy jets plus missing transverse energy. The analysis of the excess in this channel can give us information on the SUSY spectrum responsible for the signal, or more exactly on the gluino and first generation squarks. The main observable for this at LHC7 is the "effective mass" M_{eff}, defined as

$$M_{\text{eff}} \equiv \sum_i p_T^i + \not{E}_T, \tag{1}$$

where the sum of transverse momenta runs on the four most energetic jets in the event. It has been shown that the peak of the M_{eff} distribution is correlated to the mass of the parent SUSY particles produced in the initial hard scattering, in particular to the mass parameter M_{SUSY}, defined as $M_{\text{SUSY}} \equiv \min(m_{\tilde{g}}, m_{\tilde{q}})$. It results that typically $M_{\text{eff}}^{\text{peak}} \simeq 1.6 \times M_{\text{SUSY}}$ [11, 12], so that the M_{eff} distribution can be used to extract information on the mass scale of the SUSY particles produced at the LHC. As we are going to discuss, this in combination with the information from indirect SUSY searches can be crucial to constrain the parameter space in case of a positive signal of SUSY is observed at LHC7.

3 Models

3.1 CMSSM

The first model we consider is the so-called Constrained MSSM, which assumes perfect universality of the soft-breaking terms. The CMSSM is completely defined by four new parameters and one sign: the universal scalar mass m_0, the common gaugino mass $M_{1/2}$, the universal trilinear coupling A_0, the sign of the Higgsino mass parameter μ and ratio of the two Higgs vacuum expectation values (vevs) $\tan\beta$. These parameters are specified at a large scale, which is usually taken to be the Grand Unification scale, M_{GUT}, and the low-energy SUSY spectrum is then obtained by solving the renormalisation group equations (RGEs).

As discussed in the previous section, the relevant quantities for the jets + missing energy searches at LHC are the mass of first generation squarks $m_{\tilde{q}}$ and the gluino mass $m_{\tilde{g}}$. Within the CMSSM, $m_{\tilde{q}}$ and $m_{\tilde{g}}$ are essentially governed by the high scale parameters m_0 and $M_{1/2}$ only, whilst remaining relatively insensitive to A_0, $\tan\beta$ and the sign of μ. For this reason, the hadron collider bounds on the SUSY particle masses, as well as the LHC7 discovery prospects, can be conveniently interpreted as contours in the m_0–$M_{1/2}$ plane, independent of the values of the other CMSSM parameters. In our numerical study presented in Sect. 4, we are going therefore to define a band in the m_0–$M_{1/2}$ plane to be explored at LHC7 and we study such region of the parameter space by randomly varying the remaining CMSSM parameters.

The renormalisation group (RG) running from M_{GUT} down to the electroweak scale generates a flavour structure for the sfermion masses, in the form of Minimal Flavour Violation (MFV) [13]. In this scenario, all flavour-violating terms are determined by the CKM elements and the third generation Yukawa couplings. In principle, we should also add two CP violating phases φ_μ and φ_A if μ and A_0 are complex parameters. These are usually constrained by the electric dipole moments (EDMs) of the electron and the neutron, and are studied separately in Sect. 4.1.

The CMSSM contributions to flavoured processes have two sources. First, as we have said, even though the CMSSM is completely universal at M_{GUT}, small flavour off-diagonal entries in the soft mass matrices, proportional to the fermionic Yukawa couplings, are generated through the RG evolution from M_{GUT} to low energies. This shall generate small mixings for left-handed squarks. On the other hand, we always have chargino and charged Higgs contributions with flavour transitions controlled by the CKM matrix. This means that each point on the parameter space, apart from being subject to the LHC constraints, is also subject to flavour constraints. The most important processes that the CMSSM can contribute to are BR($b \to s\gamma$) and the muon anomalous magnetic moment, $(g-2)_\mu$. Another process that is becoming very important with the improvement of the experimental constraints is $B_s \to \mu^+\mu^-$. We will discuss all these processes and how they affect the CMSSM parameter space in the next section.[2]

3.2 SUSY seesaw

As widely discussed in the literature, the field content of the MSSM has to be extended, in order to account for neutrino masses and mixing. Here we are going to consider the

[2] Another important constraint comes from the comparison of the predicted dark matter abundance, assuming it is given by the neutralino, with the observed value by the WMAP experiment, as well as from direct and indirect dark matter searches. For recent discussions of these constraints, see [14, 15].

simplest possibility, the so-called type-I seesaw mechanism [4–7], which requires the introduction of right-handed (RH) Majorana neutrinos (N_i) in the MSSM superpotential:

$$W_{\mathrm{MSSM_{RN}}} = W_{\mathrm{MSSM}} + (Y_\nu)_{ij} N_i L_j H_u + (M_R)_{ij} N_i N_j \quad (2)$$

Since there is no gauge symmetry that protects them, the RH neutrinos can get large Majorana masses $(M_R)_{ij}$, breaking the conservation of lepton number. When integrated out, they will give rise to an effective light neutrino Majorana mass matrix:

$$m_\nu = -Y_\nu^T M_R^{-1} Y_\nu \langle H_u \rangle^2, \quad (3)$$

where $\langle H_u \rangle$ is the vev of the up sector Higgs field.

We do not expect the SUSY searches at the LHC to be considerably modified with respect to the CMSSM by RG effects induced by the presence of RH neutrinos. In fact, the gluino mass running is not modified (up to two loops) and squark masses can be affected only indirectly through modification of the RG running of A_t and $m^2_{H_u}$. However, for particular regions of the parameter space, these modifications can change the EWSB conditions.[3]

The main effect of the presence of RH neutrinos is given by the modification of the RG running of the left-handed slepton soft mass matrix $m^2_{\tilde{L}}$, such that, even starting with diagonal and universal scalar matrices at high energy, off-diagonal flavour mixing entries of $m^2_{\tilde{L}}$ are generated by the running above the RH neutrino mass scale [18]. In the basis where charged leptons are diagonal, these off-diagonal entries are approximately given by the following expression:

$$\left(m^2_{\tilde{L}}\right)_{i\neq j} \simeq -\frac{3m_0^2 + A_0^2}{8\pi^2} \sum_k (Y_\nu)^\dagger_{ik} (Y_\nu)_{kj} \ln\left(\frac{M_U}{M_{R_k}}\right), \quad (4)$$

where M_{R_k} is the mass of the kth RH neutrino, M_U the energy scale at which universality conditions are imposed (in our case the GUT scale). Terms in (4) clearly determine a misalignment among lepton and slepton mass eigenstates in the flavour space, inducing a contribution to lepton flavour violation (LFV) processes, such as $\ell_i \to \ell_j \gamma$, via slepton-neutralino (or sneutrino–chargino) loops. Therefore, in the context of a SUSY seesaw model, we can consider in addition as key observables the rates of LFV processes, which are suppressed to vanishing values within the SM (and the CMSSM). The rate for the processes $\ell_i \to \ell_j \gamma$ is given by [19]

$$\frac{\mathrm{BR}(\ell_i \to \ell_j \gamma)}{\mathrm{BR}(\ell_i \to \ell_j \nu \bar{\nu})} = \frac{48\pi^3 \alpha_{\mathrm{em}}}{G_F^2} \left(\left|A_L^{ij}\right|^2 + \left|A_R^{ij}\right|^2\right), \quad (5)$$

where the amplitudes can be easily estimated in terms of the mass-insertion parameters (MIs), as usually defined as $\delta^f_{ij} = (m^2_{\tilde{f}})_{i\neq j}/\bar{m}^2_{\tilde{f}}$ (with $\bar{m}^2_{\tilde{f}}$ being the average sfermion mass); in SUSY seesaw models the main contributions are approximately given by the following expression [20]:

$$A_L^{ij} \simeq \frac{\alpha_2}{60\pi} \frac{\tan\beta}{\tilde{m}^2} \left(\delta^e_{LL}\right)_{ij}, \quad (6)$$

where $\tilde{m}$ is the typical mass of the SUSY particles in the loop. On the other hand, the A_R^{ij} amplitudes turn out to be negligible since $(\delta^e_{RR})_{ij}$ are vanishing in SUSY seesaw models. From these equations, we can see that the ratio between the two of the most promising channels, $\tau \to \mu\gamma$ and $\mu \to e\gamma$, is given by

$$R_{\tau\mu} \equiv \frac{\mathrm{BR}(\tau \to \mu\gamma)}{\mathrm{BR}(\mu \to e\gamma)} \simeq 0.17 \times \frac{|(\delta^e_{LL})_{23}|^2}{|(\delta^e_{LL})_{12}|^2}. \quad (7)$$

It is clear that any estimate of $(m^2_{\tilde{L}})_{i\neq j}$ (and thus of $(\delta^e_{LL})_{ij}$) would require a complete knowledge of the neutrino Yukawa matrix $(Y_\nu)_{ij}$ which is not fixed by the seesaw equation, even with an improved knowledge of the neutrino oscillation parameters, as in (3) there is a mismatch between the number of unknowns and that of low energy observables. For definitiveness, we are going to study two well-motivated scenarios.

Scenario (a) In the first one we assume $Y_\nu \sim Y_u$, as expected in presence of an underlying Pati–Salam or SO(10) unification [21]. A consequence of this assumption is that at least one entry in Y_ν results in a value as large as the top Yukawas, so that sizeable LFV entries might be generated from RG evolution as in (4). However, even if the eigenvalues of Y_ν are then related to the ones of Y_u, the size of mixing angles in Y_ν are still uncertain. A way to bypass the ignorance about the mixing is considering two extremal benchmark cases [21, 22]. As a minimal mixing case we take the one in which the neutrino and the up Yukawa unify at the high scale, so that the mixing is given by the CKM matrix, in the basis where the lepton Yukawa Y_e is diagonal; we refer to this case as 'CKM-case'. As a maximal mixing scenario we take the one in which the observed neutrino mixing is coming entirely from the neutrino Yukawa matrix, so that $Y_\nu = U^\dagger_{\mathrm{PMNS}} \cdot Y_u^{\mathrm{diag}}$, where U_{PMNS} is the neutrino mixing matrix. This is what we are going to call 'PMNS-case'.

Scenario (b) The second case we are going to study can be better understood in terms of the Casas-Ibarra parametrisation [23]:

$$Y_\nu = \frac{1}{\langle H_u \rangle} \mathcal{D}_{\sqrt{M_R}} R \mathcal{D}_{\sqrt{m_\nu}} U^\dagger_{\mathrm{PMNS}}, \quad (8)$$

[3] Another consequence of introducing RH neutrinos is that this might destabilise the regions which provide a neutralino lightest supersymmetric particle consistent with the WMAP bounds on DM relic density, such as the focus point and A-funnel regions [16, 17].

Table 1 Estimated values of the LFV parameters $(\delta^e_{LL})_{ij}$ and the ratio $R_{\tau\mu}$ for different SUSY seesaw scenarios. The LH slepton masses is approximately $\bar{m}^2_{\tilde{\ell}} \simeq m_0^2 + 0.5 M^2_{1/2}$. In the $Y_\nu \sim Y_u$ scenario, the mass M_{R_3} of N_3 is given by $M_{R_3} \approx m_t^2(M_U)/4m_{\nu_1}$ (CKM case), $M_{R_3} = m_t^2(M_U)/m_{\nu_3}$ (PMNS case), where $m_t(M_U) \approx 0.5 m_t(m_t)$. In the $R = \mathbf{1}$ scenario $y_{\nu_3} = \sqrt{m_{\nu_3} M_{R_3}}/v_u$. To estimate $R_{\tau\mu}$, we take $U_{e3} \simeq 0.08$–0.28 and $m_{\nu_1} \simeq 0$–0.1 eV

Scenario		$(\delta^e_{LL})_{ij}$	$R_{\tau\mu}$
(a) $Y_\nu \sim Y_u$	CKM case	$-\frac{1}{8\pi^2}\frac{3m_0^2+A_0^2}{\bar{m}^2_{\tilde{\ell}}} y_t^2 V_{ti} V_{tj} \ln \frac{M_U}{M_{R_3}}$	$0.17 \times \lvert\frac{V_{tb}}{V_{td}}\rvert^2 \simeq 2 \times 10^3$
	PMNS case	$-\frac{1}{8\pi^2}\frac{3m_0^2+A_0^2}{\bar{m}^2_{\tilde{\ell}}} y_t^2 U_{i3} U_{j3} \ln \frac{M_U}{M_{R_3}}$	$0.17 \times \lvert\frac{U_{\tau 3}}{U_{e3}}\rvert^2 \simeq 1$–$15$
(b) $R = \mathbf{1}$	Degenerate M_R	$-\frac{1}{8\pi^2}\frac{3m_0^2+A_0^2}{\bar{m}^2_{\tilde{\ell}}} (\sum_k y^2_{\nu_k} U_{ik} U_{jk}) \ln \frac{M_U}{M_R}$	$\simeq 0.5$–10
	Hierarchical M_R	$-\frac{1}{8\pi^2}\frac{3m_0^2+A_0^2}{\bar{m}^2_{\tilde{\ell}}} y^2_{\nu_3} U_{i3} U_{j3} \ln \frac{M_U}{M_{R_3}}$	$0.17 \times \lvert\frac{U_{\tau 3}}{U_{e3}}\rvert^2 \simeq 1$–$15$

where $\mathcal{D}_{\sqrt{m_\nu}}$ and $\mathcal{D}_{\sqrt{M_R}}$ are diagonal matrices of the square roots of light and heavy neutrino masses respectively and the complex orthogonal matrix R accounts for the mismatch between seesaw and low-energy parameters. For simplicity we are going to consider $R = \mathbf{1}$, which corresponds to a trivial flavour structure of M_R, i.e. the leptonic mixing $U_{\rm PMNS}$ entirely provided by Y_ν. With this assumption, the mixing structure of Y_ν is fixed and the LFV effect of (4) depends on the overall size of the Yukawas, namely on the M_R scales. As a consequence, the experimental limits on LFV processes, such as $\mu \to e\gamma$ are going to constrain the RH mass scales. For definitiveness, we are going to consider both cases of very hierarchical and almost degenerate RH neutrinos.

In Sect. 4.2, we are going to study the interplay among SUSY searches at the LHC and searches for LFV processes (in particular $\mu \to e\gamma$ at the MEG experiment) for the two scenarios described above. In Table 1, we summarise the estimates for the LFV parameters δ^e_{ij} we can obtain from the leading-log expression of (4) in the different scenarios we are going to consider in the full numerical analysis. We also display the resulting values for the ratio $R_{\tau\mu}$ defined in (7). To estimate $R_{\tau\mu}$, we use for U_{e3} the recently reported 95% CL range of T2K $U_{e3} \simeq 0.08$–0.28 [24], and $m_{\nu_1} \simeq 0$–0.1 eV. We see that, for the cases where LFV is directly related to the $U_{\rm PMNS}$ entries, the U_{e3} values preferred by T2K make $R_{\tau\mu}$ at most of $\mathcal{O}(10)$, so that the present limit on $\mu \to e\gamma$ prevents $\mathrm{BR}(\tau \to \mu\gamma)$ to be within the future experimental sensitivity, as we are going to discuss in the numerical analysis.

3.3 A flavoured CMSSM

Although the simple structure of the soft breaking terms of the CMSSM can be found in some theoretical models, complete flavour universality of the soft SUSY breaking is a strong assumption and it is not generally realised in most of supergravity and string-inspired models of SUSY breaking. This fact encourages the evaluation of models departing from this complete flavour universality.

A completely general MSSM includes two types of departure from the CMSSM structure: (1) the non-degeneracy of flavour-blind masses for different matter representations of the gauge group ($m_{\tilde{Q}} \neq m_{\tilde{u}^c} \neq m_{\tilde{d}^c} \neq m_{\tilde{L}} \neq m_{\tilde{e}^c} \neq m_{H_1} \neq m_{H_2}$) or gaugino masses ($M_1 \neq M_2 \neq M_3$), and (2) the inclusion of more general flavour structures, i.e. different flavour off-diagonal entries in the sfermions mass matrices. Both departures would be expected in a generic MSSM, but as a first step, we consider them separately. That is, in (1) we would consider different masses for different SM representations but identical masses for the three generations, whilst in (2) we keep gaugino universality and equal soft mass matrices for different SM representation at $M_{\rm GUT}$, as could be expected if we have a GUT symmetry at higher scales.

In the first kind of deviation it is natural to expect to have a spectrum that can be very different from the one of the CMSSM. Only if the various initial values of the scalar and gaugino masses are of similar magnitude, the CMSSM spectrum might still be a good approximation of the spectrum of this generic MSSM. However, for a more general case, one has to be careful when using the ATLAS and CMS data, and establish specific bounds for each particular model. Defining such bounds is outside the scope of this work, so in the following we shall not consider MSSM models with this type of deviation.

In contrast, from the second kind of deviation one can expect a spectrum very close to that of the CMSSM. This is due to the fact that the stringent flavour-changing neutral currents (FCNC) and CPV constraints force non-degeneracy and flavour-violating entries in the sfermion mass matrices to be very small, such that these additional parameters, though important in FCNC processes, are not very relevant

for the sfermion masses themselves.[4] In this case, one can confidently apply the current ATLAS and CMS bounds on their parameter space, as they depend only on the gluino, lightest neutralino and first generation squark masses, but still get in the flavour sector a phenomenology that differs from the CMSSM expectations. This makes this sort of deviation particularly interesting for flavour physics, as one can concentrate on low-energy phenomenology without the necessity of performing a full collider simulation at the same time. We refer to any model exhibiting such kind of deviation as a "Flavoured CMSSM," and shall study a particular example further ahead.

From a theoretical point of view we consider a Flavoured CMSSM as the first step towards a more "realistic" MSSM. Indeed, flavour universality is not at all a feature of the SM Yukawa couplings and an analogous breaking of flavour universality is still allowed and should be expected in the SUSY soft breaking terms. Nevertheless, if we consider Grand Unification as a guiding principle of these models, different gaugino masses and the masses of the different SM representations are expected to unify.

Still, the main difficulty in defining a Flavoured CMSSM is to choose the flavour structure to assign to the soft-breaking terms. An attractive principle for this is to demand the mechanism that generates the structure in the observed Yukawa coupling to also generate the flavour structures in the soft-breaking terms. In this way, one can expect the structures in the latter to be related to the known Yukawa couplings. Notice that even when accepting this principle there is a host of different possibilities, simply because we do not know the full structure of the Yukawa matrices (only masses and left-handed mixing angles are observable). In the following, we shall follow this principle, and assume that the mechanism for generating flavour is based on a flavour symmetry.

The addition of a new flavour symmetry represents an interesting attempt to explain the mass hierarchies and mixings already found in nature. In the limit of the exact symmetry, under which the flavoured SM fields transform, the Yukawa couplings are usually forbidden, and need to be generated through the spontaneous breaking of the symmetry. This breaking is usually carried out through the introduction of new scalar particles, called flavons, which acquire a vev. The masses and mixings are then generated through effective couplings between the SM particles and the flavons. The hierarchy is interpreted as an effect of the ratio between the flavon vev and the scale of the operator, which acts as a suppression parameter (an incomplete list of examples can be found in [8, 26–29]).

[4] A similar approach can be found in [25], where the deviations in the diagonal elements from the CMSSM expectations are described.

In a SUSY scenario, both scalar and fermion components of the flavoured superfields transform under the new symmetry. Thus, in the same way as for the Yukawa couplings, the flavon vevs generate a structure for the flavoured soft SUSY-breaking terms. In many cases, the generated structures are suppressed enough in order to satisfy the strict bounds coming from FCNC processes, but are larger than those predicted by a MFV framework (see for instance [30]). Thus, flavour symmetry models represent a testable solution to the so-called SUSY flavour problem.

The model proposed in [29, 31] is based on an $SU(3)$ flavour symmetry, and reproduces successfully the quark and lepton masses and mixings, following the structure outlined in [32]:

$$Y_u = \begin{pmatrix} 0 & \varepsilon^3 & \varepsilon^3 \\ \varepsilon^3 & \varepsilon^2 & \varepsilon^2 \\ \varepsilon^3 & \varepsilon^2 & 1 \end{pmatrix} y_t \qquad Y_d = \begin{pmatrix} 0 & \bar{\varepsilon}^3 & \bar{\varepsilon}^3 \\ \bar{\varepsilon}^3 & \bar{\varepsilon}^2 & \bar{\varepsilon}^2 \\ \bar{\varepsilon}^3 & \bar{\varepsilon}^2 & 1 \end{pmatrix} y_b, \quad (9)$$

where $\bar{\varepsilon} = 0.15$ and $\varepsilon = 0.05$ parametrise the ratio between the flavon vevs and the scale of the effective operators. In addition, the model also solved the SUSY flavour problem, as it implied almost degenerate sfermions and small flavour-violation terms. The structures, in the basis where Y_d is diagonal, roughly followed

$$m^2_{\tilde{Q}} = \begin{pmatrix} 1+\varepsilon^2 & \varepsilon^2\bar{\varepsilon} & \bar{\varepsilon}^3 \\ \varepsilon^2\bar{\varepsilon} & 1+\varepsilon^2 & \bar{\varepsilon}^2 \\ \bar{\varepsilon}^3 & \bar{\varepsilon}^2 & 1 \end{pmatrix} m_0^2, \quad (10)$$

$$m^2_{\tilde{d}^c_R} = \begin{pmatrix} 1+\bar{\varepsilon}^2 & \bar{\varepsilon}^3 & \bar{\varepsilon}^3 \\ \bar{\varepsilon}^3 & 1+\bar{\varepsilon}^2 & \bar{\varepsilon}^2 \\ \bar{\varepsilon}^3 & \bar{\varepsilon}^2 & 1 \end{pmatrix} m_0^2. \quad (11)$$

A further expansion in [33] contemplated the spontaneous breaking of a CP symmetry, through which all phases become constrained within the flavour sector. This was shown to solve the SUSY CP problem in [34], and to help reduce the CPV tensions in the quark sector in [35, 36].

As an example of how the collider and flavour interplay works for Flavoured CMSSM models, we shall take two definite examples, taken from [35]. In Table 2 we show the order of magnitude of their mass-insertions, at the GUT scale.[5] Here, Σ_f is the ratio between the vev of a Georgi–Jarlskog field and the scale, oriented in the $(B - L + 2T_3^R)$ direction, used to differentiate between the charged lepton and down quark masses. Notice that our intention is to show the collider and flavour interplay for a Flavoured CMSSM and not

[5] The renormalisation group running down to low energy modifies the mass-insertion parameters in the following way: $\delta^f_{XY}(M_{\rm SUSY}) \approx \mathcal{R} \times \delta^f_{XY}(M_{\rm GUT})$, with $\mathcal{R} \approx m_0^2/(m_0^2 + 0.5M^2_{1/2})$ ($\approx m_0^2/(m_0^2 + 0.15M^2_{1/2})$) for δ^e_{LL} (δ^e_{RR}) and $\mathcal{R} \approx m_0^2/(m_0^2 + 6M^2_{1/2})$ for the hadronic mass-insertions.

Table 2 Magnitude of mass-insertions in the considered models, at the GUT scale. Here $\varepsilon = 0.05$, $\bar{\varepsilon} = 0.15$ and $\Sigma_e = 3\Sigma_d$

	$\lvert(\delta^{d,e}_{LL})_{12}\rvert$	$\lvert(\delta^{d,e}_{LL})_{13}\rvert$	$\lvert(\delta^{d,e}_{LL})_{23}\rvert$	$\lvert(\delta^{d,e}_{RR})_{12}\rvert$	$\lvert(\delta^{d,e}_{RR})_{13}\rvert$	$\lvert(\delta^{d,e}_{RR})_{23}\rvert$	$\lvert(\delta^{u}_{RR})_{12}\rvert$	$\lvert(\delta^{u}_{RR})_{13}\rvert$	$\lvert(\delta^{u}_{RR})_{23}\rvert$
Model 1	$\frac{1}{\Sigma_f}\varepsilon^2\bar{\varepsilon}$	$y_t\bar{\varepsilon}^3$	$\Sigma_f y_t\bar{\varepsilon}^2$	$\frac{1}{\Sigma_f}\bar{\varepsilon}^3$	$\frac{1}{\Sigma_f}\bar{\varepsilon}^3$	$\bar{\varepsilon}^2$	$\frac{1}{\Sigma_u}\varepsilon^3$	$y_t\varepsilon^3$	$\Sigma_u y_t\varepsilon^2$
Model 2	$\frac{1}{\Sigma_f}\varepsilon^2\bar{\varepsilon}$	$\frac{1}{\Sigma_f}\sqrt{y_t}\varepsilon\bar{\varepsilon}$	$\sqrt{y_t}\varepsilon$	$\frac{1}{\Sigma_f}\bar{\varepsilon}^3$	$\frac{1}{\Sigma_f}\sqrt{y_b}\bar{\varepsilon}^2$	$\sqrt{y_b}\bar{\varepsilon}$	$\frac{1}{\Sigma_u}\varepsilon^3$	$\frac{1}{\Sigma_u}\sqrt{y_t}\varepsilon^2$	$\sqrt{y_t}\varepsilon$

Table 3 EW scale CKM parameters used in the fit

λ	A	$\bar{\rho}$	$\bar{\eta}$
$0.22535 \pm .00065$	0.804 ± 0.010	0.111 ± 0.07	0.381 ± 0.03

to study the exact details of these models. Further details of the models can be found in [37], as well as the original references.

In terms of the size of the mass-insertions, the main difference between the MFV framework and these models is the existence of a sizeable δ_{RR}. This fact, as well as the large leading-order phases, motivate us to include these models within our analysis. Moreover, as they are meant to be embedded within a GUT framework, the flavour structures of the squark and slepton sectors are related. This means that interesting correlations, unavailable in the MFV framework, might arise.

In the following analysis, we shall include both example models. Our strategy will similar to that for the CMSSM analysis, with the following exceptions: for each point in the parameter space, we vary the $\mathcal{O}(1)$ terms randomly between 0.5 and 2 (with arbitrary sign). In addition, as the flavon phases in the soft terms are related to the phases in the Yukawas, we perform a fit of all parameters entering the Yukawas at the GUT scale, using the masses and CKM parameters at that scale as constraints. The electroweak scale CKM parameters are taken from the Tree Level fit of [38], and are shown in Table 3. After the fit, we run each point down to the electroweak scale with two-loop Renormalisation Group Equations (RGEs), using a modified version of SPheno3.1.4 [39, 40]. SPheno then calculates the threshold corrections to the Yukawas, obtaining tree-level Yukawas, which are later used to re-fit the parameters. As the tree-level Yukawas are dependent on the point of the parameter space, we need to perform an independent GUT-scale fit for every point in our scan. We do this such that the most general sample of phases compatible with the CKM structure is obtained.

As these models present a richer phase structure than the CMSSM, in addition to the observables mentioned in the previous sections, we shall also check whether the CPV tension in the $\varepsilon_K - S_{\psi K_s}$ sectors is ameliorated. Furthermore, we shall show the size of the $S_{\psi\phi}$, as well as the EDMs of both the electron and the neutron. All of these observables shall be briefly explained in further sections.

4 Interplay of LHC with flavour experiments

4.1 CMSSM

Our starting point in the analysis is assuming that an excess will be found at LHC7 in the jets plus missing energy channel, which should correspond to the production of new coloured particles. The information we will have from LHC measurements will be the number of non-SM events and some information on M_{eff} and $\not{E}_T$.

In an MSSM context, the produced SUSY particles can be mostly a pair of first-generation squarks, a gluino pair or a squark-gluino pair. As discussed in Sect. 2, the cross section is basically fixed by the superpartner masses. In fact, if we are able to observe an excess in the jets plus missing energy channel with a certain amount of integrated luminosity, one can find an upper limit on the produced SUSY particle mass, and this translates in a well-defined region in the m_0–$M_{1/2}$ plane. The lower edge of this region is set by the present bounds from non-observation of SUSY particle at LEP and Tevatron experiments together with the recent results from ATLAS and CMS with 1 fb^{-1}. The upper edge can be obtained by simulations of the number of signal and background events expected at LHC7 with the assumed integrated luminosity. Throughout this analysis, we make use of the results of [10] to estimate the LHC reach with a luminosity of 5 fb^{-1}.[6] We have chosen this integrated luminosity as a conservative measure for the 7 TeV run, considering that at the moment there is a possibility of increasing the collider energy by 2012.

Thus, we assume that the band in the m_0–$M_{1/2}$ plane, as defined above, represents the region of the CMSSM parameter space that will be explored by the LHC experiments during this $\sqrt{s} = 7$ TeV run and we study it by means of the code SPheno [39, 40]. Within this band, gluino masses span values between 560 and 1350 GeV, whilst the masses of the heaviest squarks (which generally correspond to the first generation) are in the 1–3.5 TeV range.

In Fig. 1, we show the explored region in the m_0–$M_{1/2}$ plane, with dashed contours corresponding to different values of $M_{\text{SUSY}} \equiv \min(m_{\tilde{g}}, m_{\tilde{q}})$. The solid contours represent

[6] In practice, we made an extrapolation of the estimated 2 fb^{-1} reach of [10], based on an analysis of the total production cross section of coloured SUSY particles at LHC7 by means of the routine PROSPINO 2.0 [45]. Moreover, we have checked that points in this region are indeed observable with 5 fb^{-1}.

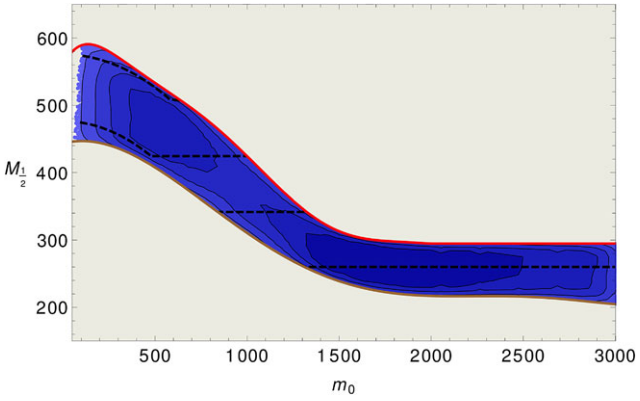

Fig. 1 (Color online) Area in the m_0–$M_{1/2}$ plane to be explored at LHC with 5 fb^{-1} integrated luminosity at 7 TeV. The *brown line* indicates the current constraints from direct searches, whilst the red line shows our estimate for the reach. The *black, dashed lines* are contours of $M_{\rm SUSY}$, as defined in the text, with values $M_{\rm SUSY} = 650, 850, 1050, 1250$ GeV from bottom to top. *Coloured contours* indicate the density of points

the density of allowed points, with the darkest colours representing a larger number of points. We show these contours to give the reader an idea of how much populated a particular region is, and do not intend to give any statistical significance to each contour. In this way, we differentiate our philosophy from that of fitting collaborations (for example [41–44]): in our point of view, every single point surviving the imposed bounds is equally valid.

The only constraints imposed in Fig. 1 are the SUSY and Higgs direct search constraints, together with the requirements of correct EWSB, absence of tachyons and neutral LSP. From the coloured contours, we see a region of intermediate m_0–$M_{1/2}$ slightly disfavoured by light Higgs searches. Two other regions, one with very large and one with very low m_0, are also slightly disfavoured, this time respectively by EWSB and neutral LSP requirements. Notice that we are only plotting the possible values of m_0 and $M_{1/2}$. The remaining CMSSM parameters, $\tan\beta$, A_0 and $\mathrm{sgn}(\mu)$ are unbounded by the considered LHC searches, although they are affected by the Higgs and EWSB constraints. For them, we take the usual ranges, $5 \leq \tan\beta \leq 55$, $-3m_0 < A_0 < 3m_0$ and $\mathrm{sgn}(\mu)$ positive.

4.1.1 *Flavour constraints: $b \to s\gamma$ and $(g-2)_\mu$*

Indirect searches of SUSY in low energy FCNC experiments provide very stringent constraints in the MSSM parameter space. Even in the CMSSM where the only non-trivial flavour structures are the usual Yukawa couplings, the experimental results are sensitive to supersymmetric contributions with CKM mixings. The main observables in this context are $\mathrm{BR}(b \to s\gamma)$ and the muon anomalous magnetic moment $a_\mu \equiv (g-2)_\mu/2$. Another interesting process is $B_s \to \mu^+\mu^-$ which is becoming more and more constraining because of the dedicated searches at LHCb and CMS [46]. Another important observable, although less restrictive at present, is $R(B^+ \to \tau^+\nu) \equiv \mathrm{BR}(B^+ \to \tau^+\nu)/\mathrm{BR}(B^+ \to \tau^+\nu)^{\rm SM}$. The main constraints we impose (including those that are relevant in the seesaw and Flavoured CMSSM models) are shown in Table 4.

The $b \to s\gamma$ process in the CMSSM receives contributions from chargino–stop loops and from charged Higgs–top loops.[7] The expressions for these supersymmetric contributions are well-known in the literature (e.g. in [59]). In the numerical analysis we use the SPheno prediction for the decay, which contains NLO expressions for MSSM contributions and NNLO contribution for the Standard Model.

The charged Higgs and the SM W-boson contributions have the same sign and interfere always constructively. In contrast, chargino contribution can have either sign depending on the sign of the Higgsino mass parameter μ. The relative sign of the chargino mediated diagram is given by $\mathrm{sgn}(A_t\mu)$. Since, in the CMSSM, A_t tends to be driven to negative values at low energies by the gluino contribution in the RGEs, $\mu > 0$ implies destructive interference, unless the initial condition A_0 is large and positive. Conversely, $\mu < 0$ usually implies constructive interference of the chargino contribution. It is also important to remember that the chargino contribution increases with the value of $\tan\beta$. Therefore, for $\mu > 0$ and large $\tan\beta$, the chargino contribution, which has opposite sign to the SM contribution, can be sizeable. Taking into account that the SM prediction is in the lower part of the experimentally allowed range, this constraint requires relatively heavy supersymmetric masses unless this contribution is compensated by a sizeable charged Higgs contribution. Therefore, we find that a supersymmetric spectrum accessible at LHC with 5 fb^{-1} tends to prefer also a not too heavy charged Higgs, $m_{H^\pm} \lesssim 1$ TeV, when A_t is large and negative ($A_t \lesssim -500$ GeV).

Similarly, in SUSY theories, a_μ receives contributions via vertex diagrams with $\tilde\chi^0$–$\tilde\mu$ and $\tilde\chi^\pm$–$\tilde\nu$ loops [60]. The chargino diagram usually dominates in most of the parameter space. The dominant $\tan\beta$ enhanced contribution approximately reads

$$\delta a_\mu \approx \frac{g_2^2}{32\pi^2}\frac{m_\mu^2}{m_{\tilde\nu}^2}\frac{\mathrm{Re}(\mu M_2)\tan\beta}{m_{\tilde\nu}^2}. \tag{12}$$

The most relevant feature of (12) is that the sign of δa_μ is fixed by $\mathrm{sgn}[\mathrm{Re}(\mu M_2)]$.

The latest experimental measurement of a_μ presents a 3σ discrepancy with the theoretical expectations in the SM [61],

[7] We recall that in presence of large flavour mixing in the squark sector, squark–gluino loops can also be important. This is the case of the Flavoured CMSSM models we are going to study below.

Table 4 Flavour constraints imposed throughout our analysis. We show only the experimental errors

$\mathrm{BR}(b \to s\gamma)$	$(3.55 \pm 0.25) \times 10^{-4}$	[47]	$\mathrm{BR}(\mu \to e\gamma)$	$<2.4 \times 10^{-12}$	[48]
$\mathrm{BR}(B_s \to \mu^+\mu^-)$	$<1.08 \times 10^{-8}$	[46]	$\mathrm{BR}(\tau \to e\gamma)$	$<3.3 \times 10^{-8}$	[49]
$R(B^+ \to \tau^+\nu)$	1.57 ± 0.53	[36, 50]	$\mathrm{BR}(\tau \to \mu\gamma)$	$<4.4 \times 10^{-8}$	[51]
$\delta a_\mu \equiv (a_\mu - a_\mu^{\mathrm{SM}})$	$(2.61 \pm 0.8) \times 10^{-9}$	[52]	ε_K	$(2.228 \pm 0.011) \times 10^{-3}$	[53]
$S_{\psi K_s}$	0.673 ± 0.023	[53]	$S_{\psi\phi}$	0.13 ± 0.19 [54] -0.55 ± 0.38 [55]	
Δm_B	$(3.337 \pm 0.033) \times 10^{-13}$ GeV	[53]	Δm_{B_s}	$(117.0 \pm 0.8) \times 10^{-13}$ GeV	[56]
d_n	$<2.9 \times 10^{-26} e$ cm^{-1}	[57]	d_e	$<2 \times 10^{-27} e$ cm^{-1}	[58]

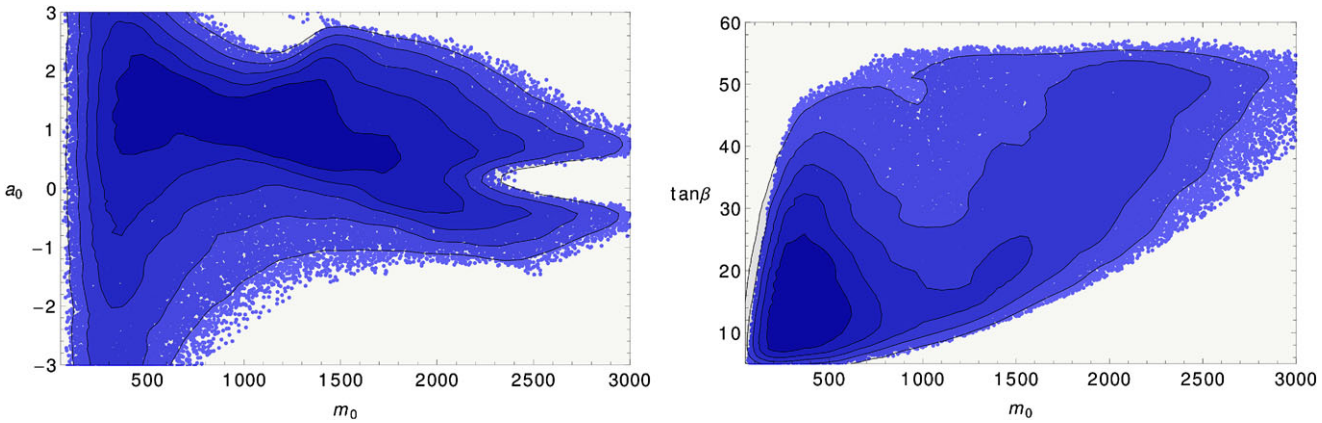

Fig. 2 Area in the m_0–a_0 (*left*) and m_0–$\tan\beta$ planes (*right*) to be explored at LHC with 5 fb^{-1} integrated luminosity at 7 TeV

as can be seen in Table 4. Therefore, at present, a positive contribution δa_μ from slepton loops at the level of $\sim 10^{-9}$ is required and so, this result strongly favours the $\mu > 0$ region in an MSSM scenario.

If we impose the $b \to s\gamma$ and δa_μ constraints at the 3σ level the allowed region is modified, with the appearance of correlations with specific values of $\tan\beta$ and A_0. If we restrict ourselves to the m_0–$M_{1/2}$ plane, we shall not find large differences with respect to Fig. 1, apart from a decrease in the density of points, particularly for large m_0. However, when examining the other planes, we find that the parameter space, although still big, is not so arbitrary anymore. We can see this directly in Fig. 2.

On the left panel of Fig. 2, we show the m_0–a_0 plane, where $a_0 \equiv A_0/m_0$. In this plane, we first see strong constraints due to EWSB and tachyons at large values of m_0 and $|a_0|$. These strong constraints are also applied for large values of m_0, when $a_0 \sim 0$. For large, positive values of a_0, we see a small, semi-circular excluded region, where the Higgs mass becomes too light. We also see a preference in the density of points disfavouring negative a_0. In these cases, the chargino contribution to $b \to s\gamma$ becomes too large, whilst for positive a_0 it has just the right size to be compensated by the charged Higgs contribution.

On the right panel of Fig. 2 we show the m_0–$\tan\beta$ plane. The two most important constraints can be seen for large m_0, low $\tan\beta$, and for low m_0, large $\tan\beta$. The first one is due to a_μ, where the SUSY contribution is not large enough to account for the anomaly. The second one corresponds to a neutral LSP. In addition, we get a significant reduction in the density of points for intermediate m_0 and large values of $\tan\beta$. Here, the $b \to s\gamma$ constraint rules out many points, as the chargino contribution again becomes too large.

4.1.2 $B_s \to \mu^+\mu^-$ bounds and prospects

In parallel with the direct searches ongoing at the ATLAS and CMS experiments, we can also expect improvements in measurements of flavour-violating observables during the 7 TeV LHC run. In particular, the LHCb experiment is designed for precision B-physics studies. Of particular interest is the decay $B_s \to \mu^+\mu^-$.

In the CMSSM, the main NP contributions to the $B_s \to \mu^+\mu^-$ branching ratio are due to neutral heavy-Higgs mediated diagrams. The amplitude then acquires a $\tan^3\beta$ dependent contribution which, as for $b \to s\gamma$, is also proportional to $A_t\mu$.

This particular decay is of great interest at the times of the LHC. Although currently the LHC has only placed upper bounds on the branching ratio of this decay channel, as shown in Table 4, both the CMS and LHCb experiments shall be able to probe its value down to that of the SM

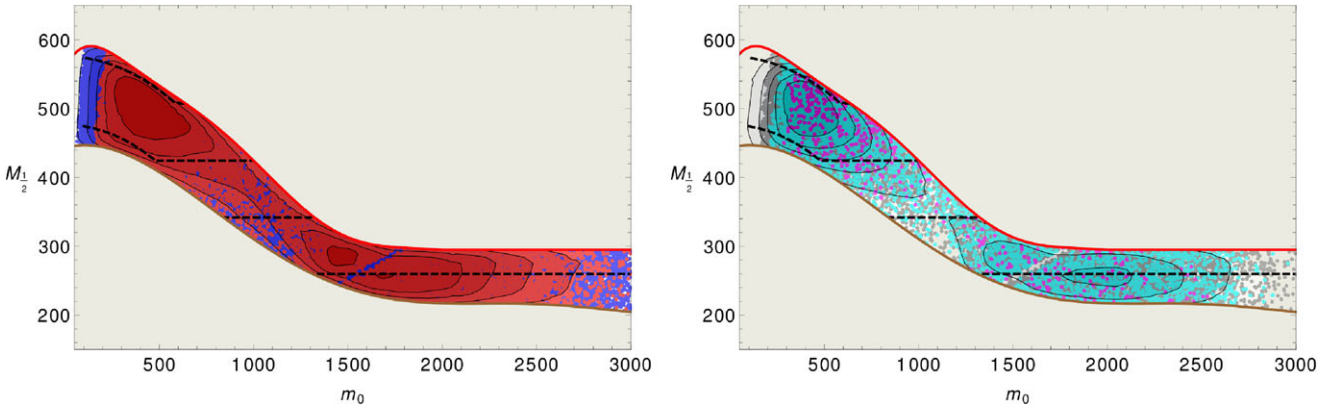

Fig. 3 (Color online) $B_s \to \mu\mu$ signal in the m_0–$M_{1/2}$ plane. *On the left*, we show in *red* (*blue*) the points with a branching ratio larger (*lower*) than 4×10^{-9}. *On the right*, we show in *magenta*, *cyan* and *grey* the points with a branching ratio larger than 9×10^{-9}, 5×10^{-9} and 4×10^{-9}, respectively

$\sim 3 \times 10^{-9}$. It is then particularly interesting to ask what would be the consequences if this particular decay is or is not observed. In particular, from a projection using 37 pb^{-1} of data [62], LHCb claims that, after collecting an integrated luminosity of 2 fb^{-1}, it would be able to achieve a 5σ discovery for a branching ratio larger than 9×10^{-9}, or find 3σ evidence for a branching ratio larger than 5×10^{-9}. In the case of not seeing any signal, the same experiment claims to be able to rule out any branching ratio larger than 4×10^{-9} with 95% confidence.[8]

The possibility of observing a large branching ratio for this decay should be taken seriously, as last summer CDF published a new analysis with a positive signal $\mathrm{BR}(B_s \to \mu^+\mu^-) = (1.8^{+1.1}_{-0.9}) \times 10^{-8}$ [64]. Notice that this signal is still compatible at 1σ with the upper bound of CMS and LHCb. We shall see that taking the central value of this positive signal at 1σ would strongly restrict our parameter space, but at the 2σ level it has practically no effect at all in our results. We hope this very intriguing situation is clarified in the near future with further analysis at CDF/D0 and CMS/LHCb.

In Figs. 3 and 4 we plot how the parameter space would be affected by an observation of $B_s \to \mu^+\mu^-$. In both figures, we plot on the left in red those points that predict a branching ratio larger than 4×10^{-9}, and would thus be ruled out if LHCb does not see any signal for this decay with 2 fb^{-1}. We leave all points with a smaller branching ratio in blue (notice that in Figs. 3 and 4 there is an overlap between blue and red points). On the right part of each figure, we plot in magenta (cyan) the points that would give a 5σ discovery (3σ evidence), and leave in grey those that would give a weaker signal.

From the figures, we see that, at this level, the observation of $B_s \to \mu^+\mu^-$ would not be crucial in the determination of m_0, $M_{1/2}$ or a_0, but could give an indication about the preferred regions of the parameter space. Larger values for the branching ratio tend to occur for positive values of a_0, since it turns out that equivalent points with negative values of a_0 are in conflict with $b \to s\gamma$. The reason is traced back to the correlation between the dominant Higgs-mediated contribution to $B_s \to \mu^+\mu^-$ and the stop-chargino contribution to $b \to s\gamma$. Points with a negative a_0 tend to give a large negative A_t, for which a sizeable $\mathrm{BR}(B_s \to \mu^+\mu^-)$ is possible, but we get in turn a too large negative stop-chargino contribution to $b \to s\gamma$, which provides a value for the branching ratio below the experimental lower bound. $B_s \to \mu^+\mu^-$ gives also very important information about the value of $\tan\beta$. Depending on the significance of the observation, along with the value of m_0, one can set a lower bound on the value of $\tan\beta$, favouring always values above 25.

One can see more clearly the interplay between the collider and flavour observables by requiring stronger constraints on the latter. For instance, we can demand each point to satisfy flavour constraints at 2σ, and, depending on what LHCb sees, ask for a $B_s \to \mu^+\mu^-$ signal of significance larger than 3σ, or no signal at all. In Fig. 5 we see the consequences of these requirements, with the upper plots corresponding to having at least a 3σ $B_s \to \mu^+\mu^-$ observation, whilst the lower plots correspond to not observing a signal at all. These figures show how the LHCb study of $B_s \to \mu^+\mu^-$, combined with the ATLAS/CMS results, can help to identify preferred regions in the SUSY parameter space.

The main conclusion from Fig. 5 is that having a 3σ evidence for $B_s \to \mu^+\mu^-$ decay will most likely rule out a significant number of points with low values of m_0. In addition, $\tan\beta$ would be forced to remain large, and a_0 would only be positive. On the other hand, a lack of observation of $B_s \to \mu^+\mu^-$ would heavily disfavour points

[8] For a study of the impact of the recent $B_s \to \mu^+\mu^-$ searches on various SUSY scenario and the discovery prospects, see also [63].

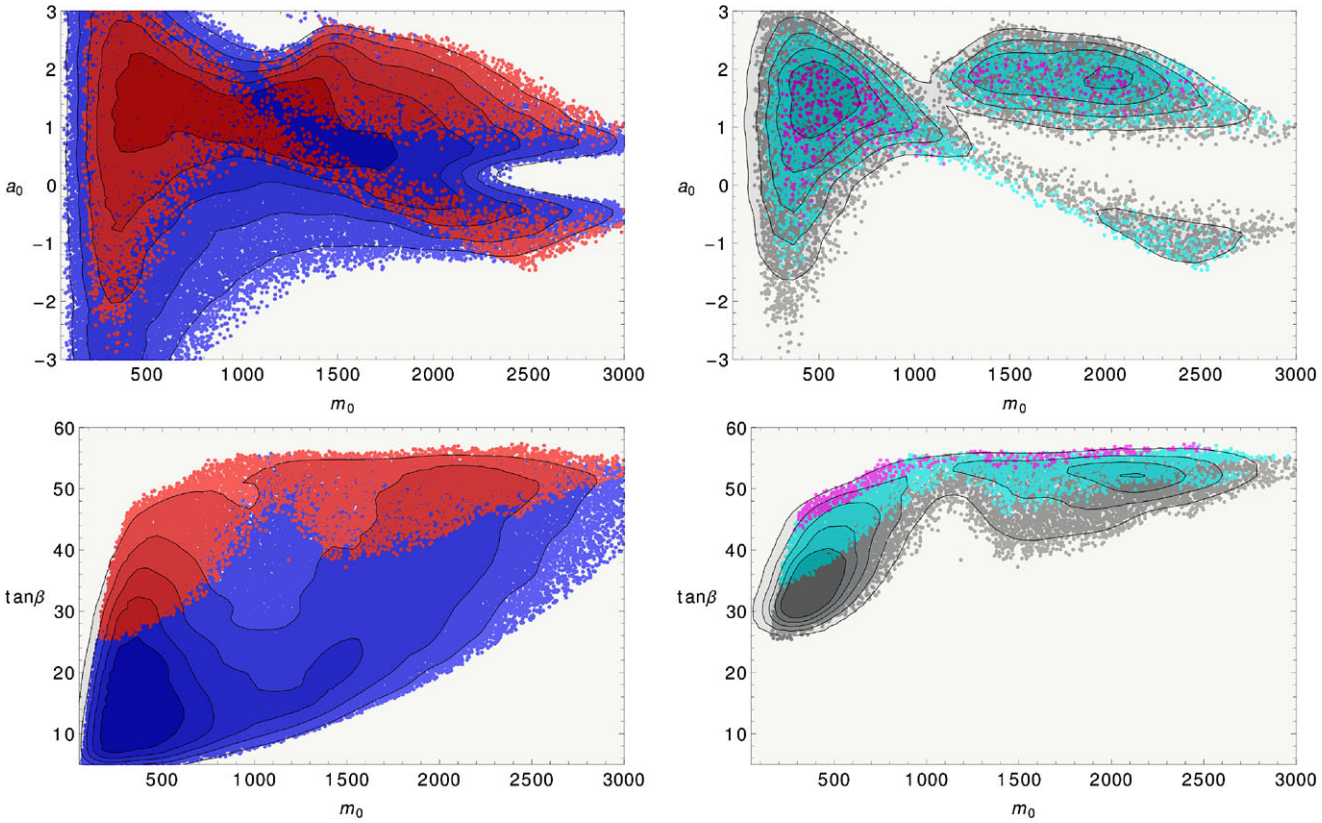

Fig. 4 As in Fig. 3, but for the m_0–a_0 (*upper*) and m_0–$\tan\beta$ (*lower*) planes

with large m_0, although it would not discard them completely. Also, a_0 would remain unfortunately unbounded (with a slight preference for large, positive values), whilst $\tan\beta$ would be preferred small, unless m_0 becomes large.

In the case where $B_s \to \mu^+\mu^-$ provides a significant signal, the correlation with $M_{\rm SUSY}$ (and thus $M_{\rm eff}$) would be a crucial check to determine if our signal is really due to SUSY. A $M_{\rm SUSY}$ lower than 850 GeV or larger than 1250 GeV would be incompatible with the observation of this process. In the case of no signal we can only make such a statement for low $M_{\rm SUSY}$, but, in addition, the correlation with this observable would help disentangle the more populated, low m_0 region from the less dense, medium m_0 region.

4.1.3 Bounds from electric dipole moments on the CPV phases

The EDM of a fermion is the coupling constant related to a P- and T-violating interaction with a photon. As for LFV decays, the EDM of a particle like the electron (d_e) or the neutron (d_n) is vanishingly small in the SM, becoming thus an excellent probe of NP. Due to its CP violating nature, an EDM is connected to phases, and the non-observation of the former becomes an important constraint on the size of the latter. Currently, the strongest constraints come from thallium [58] (related to that of the electron), mercury [65] and the neutron [57] (both related to quarks).

In the MSSM, we find that the six relevant flavour-independent phases are related to the following invariants [66, 67]:

$$\arg\bigl(A_f^* M_i\bigr), \quad \arg\bigl((B\mu)^* \mu A_f\bigr), \tag{13}$$

where $i = 1, 3$ and $f = u, d, e$. It is common to take the convention where $B\mu$ and the gluino mass M_3 are real parameters. Moreover, if gaugino universality is invoked, we can eliminate two further phases, and have only a phase for μ and a global phase for each A_f.

Further complex invariants can appear if one allows flavour-violating terms. For example, if one takes into account δ^f_{LL} and δ^f_{RR} insertions, it is possible to construct the following invariants [68, 69]:

$$\arg\bigl(Y_f\bigl[Y_f^\dagger Y_f, \delta^f_{LL}\bigr]\bigr), \tag{14}$$

$$\arg\bigl(\delta^f_{RR} Y_f Y_f^\dagger Y_f\bigr), \tag{15}$$

$$\arg\bigl(\delta^f_{LL} Y_f \delta^f_{RR}\bigr). \tag{16}$$

The dominance of one invariant over the other, may them be flavour-dependent or independent, is determined by the underlying flavour structure of the model. For instance, in the CMSSM, the δ^f_{RR} insertions vanish and the δ^f_{LL} phases

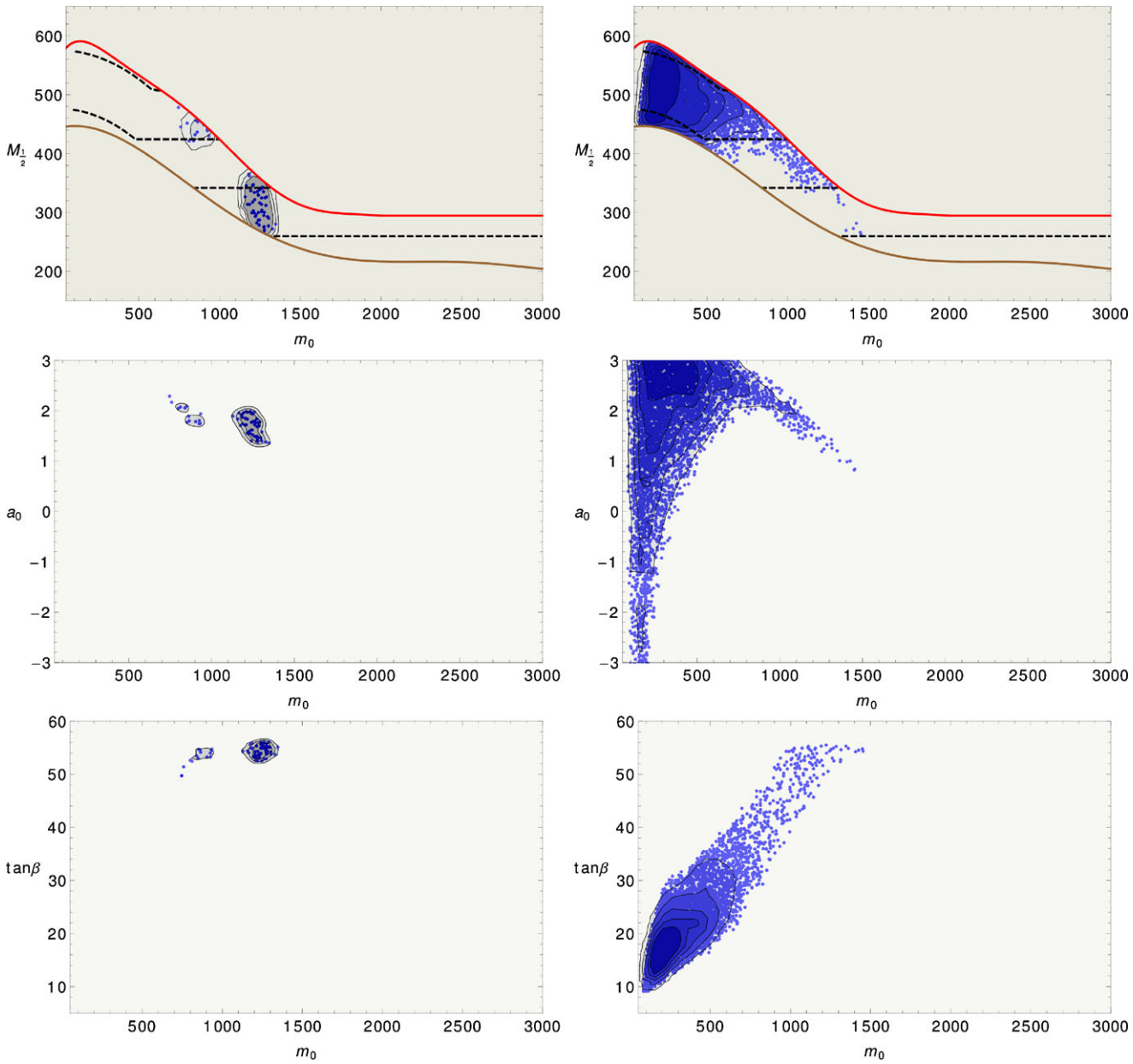

Fig. 5 Points in the parameter space satisfying experimental 2σ constraints. *The plots on the left column* are associated with a 3σ evidence signal of $B_s \to \mu^+\mu^-$ decay at LHCb with 2 fb^{-1} of data, whilst the *right column* predict no such signal. We show the m_0–$M_{1/2}$, m_0–a_0 and m_0–tan β planes on the *top*, *middle* and *bottom rows*

are small, such that the main contribution to EDMs shall come from the flavour-independent terms. In contrast, in the flavour models we are taking as examples of a Flavoured CMSSM, flavour-independent phases are forbidden, whilst sizeable δ^f_{RR} are available, meaning that the only contributions to EDMs shall be those of the second type. For more details on the SUSY contributions to the EDM of the electron and neutron, for these models, we refer the reader to [34, 35].

For the CMSSM with and without right-handed neutrinos, it is possible to use d_e to directly place upper bounds on the imaginary part of μ and A_e at the EW scale. For d_n, as the prediction of the EDM depends on the neutron model one uses, the establishment of bounds is not so straightforward. In the following, we shall use the quark-parton (QP) [70] and chiral quark (CQ) [71] models for d_n. By considering these models, it is possible to establish further bounds on the imaginary part of μ, and new bounds on those of A_u and A_d.

Using only the points that survive direct search, Higgs search and flavour 3σ constraints, we have calculated the upper bound on the phases of μ (δ_μ) and the global phases of

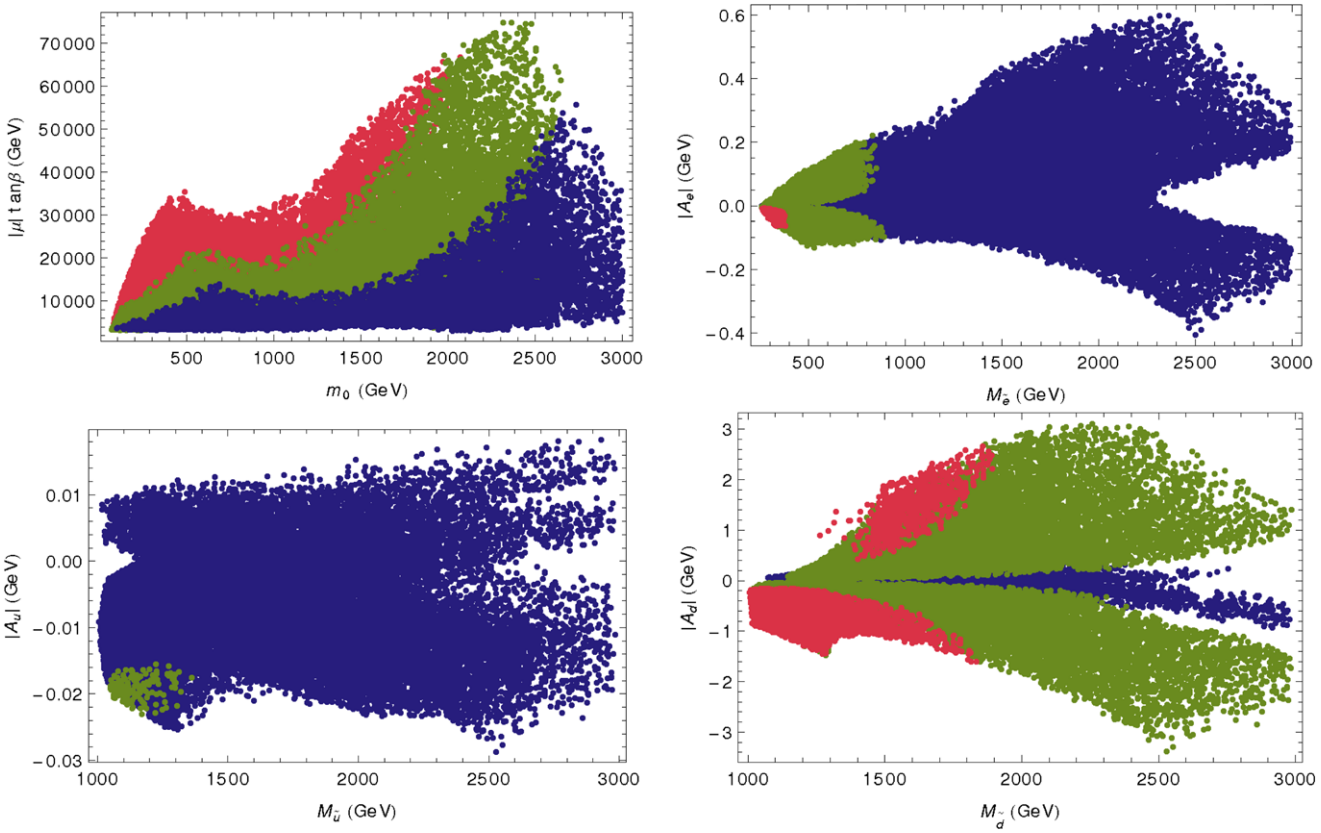

Fig. 6 From left to right, top to bottom, upper bounds on the global phase of μ, A_e, A_u and A_d at the electroweak scale. For the trilinears, we specify the sign of their real part. The text explains the meaning of the colours

A_f terms (δ_{A_f}). Our results are shown in Fig. 6. The upper left panel shows the values of δ_μ in the $|\mu|\tan\beta - m_0$ plane. We see in red the points where $\sin\delta_\mu < 5\times10^{-3}$, in green those where $\sin\delta_\mu < 10^{-2}$ and in blue those points where the phase can be larger. Within the data, we find a maximum possible phase $\sin\delta_\mu^{\max} = 0.02$ rad.

The upper right panel shows the values of δ_{A_e}, in the $|A_e|$–$M_{\tilde{e}}$ plane. Here, all blue points are unconstrained by the EDM data. The green points have $0.1 < \sin\delta_{A_e} < 1$, whilst the red points must have smaller values. We do not find any phase constraint smaller than 5×10^{-2}. We find that the constraints are weaker than those on the phase of μ. This is due to the $\tan\beta$ enhancement that the μ-insertion receives, as well as to an additional chargino contribution dependent on the imaginary part of μ. Of course, as the EDM is proportional to the imaginary part of A_e, the size of its absolute value after the RG running also plays a role on how much the phase is constrained.

The lower left panel shows the constraints on δ_{A_u}, in the $|A_u|$–$M_{\tilde{u}}$ plane. Again, the blue points are unconstrained, whilst the green points have some weak upper bound for $\sin\delta_{A_u}$, all of them larger than 0.5. Here we find that the absolute value of A_u after the running is smaller than that for A_e, so it is reasonable to find even weaker constraints than in the former case.

Finally, the lower right panel shows the constraints on δ_{A_d}, in the $|A_d|$–$M_{\tilde{d}}$ plane. This time, as the average size of $|A_d|$ is larger, we find somewhat stronger constraints. The red points have $\sin\delta_{A_d} < 0.1$, the green points have $\sin\delta_{A_d} < 1$, and the blue points are unconstrained. The maximum bound is never lower than 10^{-2}.

To summarise, within the region accessible to LHC7 with 5 fb^{-1}, we find the requirement of a very strong suppression on the phase of μ, and a somewhat milder one for those of A_e and A_d. The phase of A_u is much less constrained. The fact that the imaginary part of most flavour independent complex parameters need to be suppressed is commonly known as the SUSY CP problem.

4.2 SUSY seesaw

We present here the results for the SUSY seesaw scenarios introduced in Sect. 3.2, starting with the $Y_\nu \sim Y_u$ case.

In Fig. 7, we plot BR($\mu\to e\gamma$) as a function of m_0 for the CKM-like (dark red) and the PMNS-like (dark green) mixing cases. All points satisfy the flavour constraints at 3σ, as in the previous section. The lighter points correspond to a

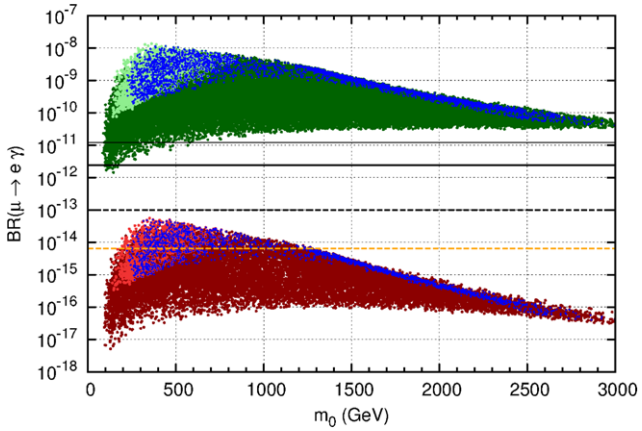

Fig. 7 (Color online) $Y_\nu \sim Y_u$ scenario: $\mathrm{BR}(\mu \to e\gamma)$ as a function of m_0 for the CKM (*red*) and the PMNS (*green*) case

contribution to a_μ, which lowers the tension with the experiments below the 1σ level. The blue points provide a sizeable $\mathrm{BR}(B_s \to \mu^+\mu^-)$, such that a 3σ evidence for such a decay is expected to be found at LHCb in the upcoming months ($\mathrm{BR} \gtrsim 5 \times 10^{-9}$). The thick horizontal line represents the current best limit recently published by the MEG experiment, $\mathrm{BR}(\mu \to e\gamma) < 2.4 \times 10^{-12}$ at 90% CL [48] (for comparison we display the previous limit 1.2×10^{-11} as well [72]). The black dashed line represents the expected final sensitivity of MEG, $\sim 10^{-13}$. The meaning of the orange dashed line will be explained below.

From the figure, we see that, within the parameter space region accessible to LHC7, the PMNS case seems to be completely ruled out by the recent MEG analysis. This is a consequence of the large eigenvalue (we recall that in both cases $y_{\nu_3} \simeq y_t$ at the GUT scale) and the large mixing angles in the neutrino Yukawa matrix. From Table 1, we see that in the PMNS case we have a dependence of $\mathrm{BR}(B_s \to \mu^+\mu^-)$ on U_{e3}. For the plot in Fig. 7, we used a value of U_{e3} in the lower side of the range preferred by recent T2K results, $U_{e3} = 0.08$. If U_{e3} will turn out to be smaller (but non-vanishing), we can still conclude that most of the parameter space in the PMNS case either is excluded or can be tested soon at MEG (we recall that in this case $\mathrm{BR}(\mu \to e\gamma) \propto |U_{e3}|^2$).[9]

On the contrary, the CKM case seems to escape the future MEG sensitivity. This is a consequence of the small mixing angles in the Y_ν combined with the present LHC bound on SUSY particle masses, which leads to already quite heavy sleptons and gauginos within models with CMSSM-like boundary conditions. There is however a way to test LFV in the μ–e sector beyond the sensitivity of MEG in the next years. This is represented by experiments searching for $\mu \to e$ conversion in nuclei. We recall that, within SUSY models, there is typically a striking correlation between $\mu \to e\gamma$ and the $\mu \to e$ conversion in nuclei, namely the $\mu \to e$ conversion rate is well approximated by

$$\mathrm{CR}(\mu \to e \text{ in N}) \simeq \alpha_{\mathrm{em}} \times \mathrm{BR}(\mu \to e\gamma). \tag{17}$$

This means that our prediction for $\mathrm{BR}(\mu \to e\gamma)$ can be easily translated in an estimate for $\mathrm{CR}(\mu \to e \,\mathrm{in\,N})$. The proposed μ–e conversion experiments at Fermilab [74] and at J-PARC [75] aim at sensitivities below 10^{-16} on $\mathrm{CR}(\mu \to e \text{ in Ti})$. In Fig. 7, we show with an orange dashed-line how a sensitivity reach on $\mathrm{CR}(\mu \to e \text{ in Ti})$ at the level of 5×10^{-17} would translate in terms of $\mathrm{BR}(\mu \to e\gamma)$, using the trivial approximation in (17). This shows that these experiments can actually access the CKM case parameter space and test at least the region favoured by a_μ (which, interestingly, might also provide $B_s \to \mu^+\mu^-$ above the SM prediction).

We now discuss the results of the numerical analysis of the scenario with $R = \mathbf{1}$ and hierarchical RH neutrinos. We varied M_{R_3} approximately in the range 3×10^{10}–3×10^{14} GeV and U_{e3} was also randomly varied within the 95% CL range recently provided by T2K, $U_{e3} \simeq 0.08$–0.28 [24].

In the left panel of Fig. 8, we plot $\mathrm{BR}(\mu \to e\gamma)$ as a function of the heaviest RH neutrino M_{R_3}. The green points gives a SUSY contribution to the muon magnetic moment $\delta a_\mu > 10^{-9}$, the blue ones correspond to $\delta a_\mu > 2 \times 10^{-9}$. We see that the present bound $\mathrm{BR}(\mu \to e\gamma) < 2.4 \times 10^{-12}$ already constrains $M_{R_3} \lesssim 6 \times 10^{13}$ GeV (with $M_{R_3} \lesssim 4 \times 10^{13}$ GeV for the blue points, for which the $(g-2)_\mu$ tension is lowered below 1σ). A negative result at MEG would further lower this bound to about $M_{R_3} \lesssim 5 \times 10^{12}$ GeV ($M_{R_3} \lesssim 2 \times 10^{12}$ GeV for the blue points). On the other hand, we see that a positive signal at MEG would constrain the third RH neutrino mass in the following range: 10^{11} GeV $\lesssim M_{R_3} \lesssim 10^{14}$ GeV (for instance $\mathrm{BR}(\mu \to e\gamma) \simeq 10^{-12}$ would imply 5×10^{11} GeV $\lesssim M_{R_3} \lesssim 5 \times 10^{13}$ GeV).

In the right panel of Fig. 8, we show $\mathrm{BR}(\mu \to e\gamma)$ vs. $\mathrm{BR}(\tau \to \mu\gamma)$ for the same scenario. As we can see, the numerical results are consistent with the estimate for the ratio of the two branching ratios, $R_{\tau\mu}$, in Table 1. As a consequence, the present bound on $\mu \to e\gamma$ already constrains $\mathrm{BR}(\tau \to \mu\gamma)$ to be at most $\mathcal{O}(10^{-10})$, beyond the sensitivity of SuperB [76] and SuperFlavour [77] factories. A positive signal for $\tau \to \mu\gamma$ at these facilities would then rule out this scenario. This is a consequence of the T2K results, which prefer quite large values of U_{e3} and disfavour scenarios with suppressed $\mathrm{BR}(\mu \to e\gamma)$ which usually require hierarchical RH neutrinos and vanishing U_{e3}.

We do not display the case with $R = \mathbf{1}$ and almost degenerate RH neutrinos, which exhibits only a mild dependence

[9] For vanishing small values of U_{e3}, on the other hand, running effects of U_{e3} itself and double mass-insertion contributions become important and still guarantee a sizeable $\mathrm{BR}(\mu \to e\gamma)$ [22, 73].

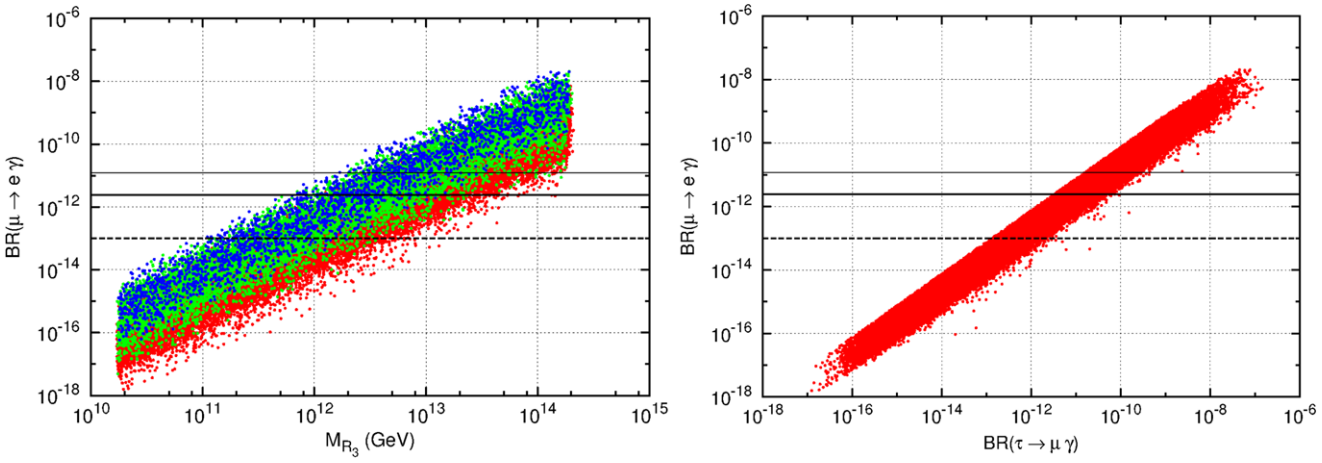

Fig. 8 (Color online) $R = \mathbf{1}$ scenario with hierarchical M_R. *Left panel*: $\mathrm{BR}(\mu \to e\gamma)$ vs. M_{R_3} (*green points* give $\delta a_\mu > 10^{-9}$, *blue points* $\delta a_\mu > 2 \times 10^{-9}$); *right panel*: $\mathrm{BR}(\mu \to e\gamma)$ vs. $\mathrm{BR}(\tau \to \mu\gamma)$

on U_{e3} (as can be easily checked by means of the expressions of Table 1) and predicts values of $\mathrm{BR}(\mu \to e\gamma)$ typically of the same order of the hierarchical case for the T2K range of U_{e3}.[10]

In models with a CMSSM-like spectrum, the mass splitting between selectrons and smuons ($\Delta m_{\tilde{\ell}}/m_{\tilde{\ell}}$) is an LHC observable directly correlated to LFV in the μ–e as well as in the τ–μ sector: $\Delta m_{\tilde{\ell}}/m_{\tilde{\ell}} \approx \max(\delta^e_{12}, \delta^e_{23}/2)$ [78]. Such an interplay has been recently addressed in the context of SUSY seesaw [79, 80]. In our set-up, the mass splitting between LH selectron and LH smuon is always small, $\Delta m_{\tilde{\ell}}/m_{\tilde{\ell}} \lesssim 10^{-3}$, as a consequence of the MEG bound and the T2K U_{e3} range, whose combination prevents $(\delta^e_{LL})_{23}$ to reach sizeable values. Even though resolving mass splitting at this level is definitively beyond the reach of LHC7, it might be possible in the future $\sqrt{s} = 14$ TeV run after some years of data taking [78, 81], provided that $\mu \to e\gamma$ is in the reach of MEG.

4.3 Flavoured CMSSM

4.3.1 Neutral meson mixing

FCNC in neutral mesons pose one of the most stringent constraints to all models beyond the SM. The accurate measurement of the mass differences in the K, D, B and B_s sector, as well as that of the CPV parameters ε_K and $\sin 2\beta$, suggest that any NP model contributing to flavour either is manifest at very high scales, or has strong flavour suppression [82].

[10] An exception is realised if the degree of degeneracy of M_{R_i} is higher than 5% and the light neutrinos are almost degenerate as well, $m_{\nu_1} \simeq 0.1$ eV. This is the only setup of the parameters for which, within the T2K range, $\mathrm{BR}(\mu \to e\gamma)$ can be suppressed with respect to the hierarchical case up to 2 orders of magnitude.

Recently, better theoretical predictions of non-perturbative parameters has lead to a small tension between ε_K, $S_{\psi K_s}$ and $\Delta m_B/\Delta m_{B_s}$ [36, 83]. In addition, evidence for a large phase on the B_s sector was reported in [84, 85], which would be related to an anomalous dimuon charge asymmetry observed at D∅ [86, 87]. Thus, it is possible that small hints in favour of NP might already be starting to appear in the flavour sector.

The relation between ε_K, $S_{\psi K_s}$ and $\Delta m_B/\Delta m_{B_s}$ can be understood most easily through the following formula [36]:

$$|\varepsilon_K|^{\mathrm{SM}} = \kappa_\varepsilon C_\varepsilon \hat{B}_K |V_{cb}|^2 |V_{us}|^2 \times \left(\frac{1}{2} |V_{cb}|^2 R_t^2 \sin 2\beta \eta_{tt} S_0(x_t) + R_t \sin\beta \left(\eta_{ct} S_0(x_c, x_t) - \eta_{cc} x_c \right) \right), \tag{18}$$

where R_t is a side of the Unitarity Triangle, defined through

$$R_t = \xi \frac{1}{\lambda} \sqrt{\frac{m_{B_s}}{m_B}} \sqrt{\frac{\Delta m_B^{SM}}{\Delta m_{B_s}^{SM}}}, \tag{19}$$

and $\sin 2\beta$ is the SM contribution to $S_{\psi K_s}$:

$$\sin(2\beta + 2\Phi_B) = S_{\psi K_s}. \tag{20}$$

Here, Δm_F^{SM} represents the SM prediction for the mass difference of the $F = B, B_s$ sectors, whilst Φ_B is a NP phase appearing in the B sector. The definition of the rest of the parameters can be found in [36], and those we use in our predictions are shown in Table 5. Thus, a fixed value of $\sin 2\beta$ and $\Delta m_B/\Delta m_{B_s}$ fixes ε_K. As can be seen in [88], if one fits the CKM parameters without taking into account ε_K, the predicted value shows a discrepancy with experiment beyond 2σ.

Table 5 Parameters used in our simulations. The B_i parameters for the SUSY contribution to our observables were taken from [97]

$\hat{B}_K$	0.724 ± 0.03	[89]	f_K	0.1558 ± 0.0017 GeV	[91]	η_{tt}	0.5765 ± 0.0065	[92]	η_B	0.551 ± 0.007	[95]
$\hat{B}$	1.22 ± 0.05	[90]	f_B	0.194 ± 0.009 GeV	[38]	η_{ct}	0.496 ± 0.047	[93]	κ_ε	0.94 ± 0.02	[96]
$\hat{B}_s$	1.28 ± 0.04	[90]	f_{B_s}	0.239 ± 0.01 GeV	[38]	η_{cc}	1.87 ± 0.76	[94]			

On the other hand, the dimuon anomaly is related to the semileptonic CP asymmetries A^d_{SL} and A^s_{SL}. The latter is in turn connected to the time-dependent CP asymmetry $S_{\psi\phi}$ through [98]

$$A^s_{SL} = -\frac{\Delta\Gamma_s}{\Delta M_{Bs}} \frac{S_{\psi\phi}}{\sqrt{1 - S^2_{\psi\phi}}} \tag{21}$$

The fit done in [99] shows that, in order to reproduce the observed anomaly, one requires both a larger Γ^s_{12} than that predicted by the SM, and a non-zero NP phase in the B_s sector, Φ_{B_s}. The latter phase is connected to $S_{\psi\phi}$ in a way analogous to (20):

$$\sin(2\beta_s - 2\Phi_{B_s}) = S_{\psi\phi}. \tag{22}$$

where $\sin 2\beta_s \approx 0.036 \pm 0.002$ is the SM prediction.[11]

The MFV contributions of the CMSSM with and without right-handed neutrinos are known to be insufficient to solve the flavour tension [101] nor the dimuon anomaly, although the latter can be slightly ameliorated in general MFV scenarios with large $\tan\beta$ and new phases [102]. If any of these models were the correct description of flavour physics in the MSSM, the tensions should disappear with inclusion of further data.

A Flavoured CMSSM, on the other hand, should be capable of providing larger contributions to FCNC. The examples mentioned in Sect. 3.3, in particular, can provide contributions to ε_K of the correct order of magnitude [35], and in some cases can even provide a large Φ_{B_s} phase [36].

Nevertheless, it turns out that the contributions to CPV observables can also exceed the requirements. In Fig. 9, we show typical values of $S_{\psi K_s}$ and ε_K for both of our examples. All points satisfy the LFV constraints, which shall be explained in detail in the next section. The dotted (dashed) lines correspond to 3σ (2σ) constraints, and include an approximate theoretical error, $\sigma^{\text{th}}_{S_{\psi K_s}} = 0.02$ and $\sigma^{\text{th}}_{\varepsilon_K} = 0.23 \times 10^{-3}$. The contours again represent a qualitative measure of the density of points, which means that one should not compare contours from different models. We see that, for ε_K, the contributions can easily exceed the 3σ bounds. Although for both models the main bulk of points is located within a region with no conflict with ε_K, there is a very large number of points where the SUSY contribution is too large. In the second example, we see that it is possible to exceed also the bounds in $S_{\psi K_s}$. This means that solving the flavour tension can become a new, important source of constraints for any Flavoured CMSSM model.

After applying the bounds on $S_{\psi K_s}$ and ε_K, one can turn to $S_{\psi\phi}$. In Fig. 10 we show $S_{\psi\phi}$ vs. $\Delta m_B/\Delta m_{B_s}$, where we have taken out all points that do not satisfy the ε_K and $S_{\psi K_s}$ constraints. The SM prediction for $S_{\psi\phi}$ at 3σ is shown by the brown dotted lines, whilst the 1σ bounds of $\Delta m_B/\Delta m_{B_s}$ are shown by the solid orange lines. We find that $\Delta m_B/\Delta m_{B_s}$ does not constrain any of the models. Notice that in the second example, although we find it is very difficult to obtain a value larger than 0.1, it is not absolutely impossible. Thus, $S_{\psi\phi}$ could be used as a tool for distinguishing between Flavoured CMSSM models, provided that the experimentally measured value is somewhat larger than that of the SM. This is expected to be probed by LHCb in the near future.

If we study both Figs. 9 and 10 at the same time, we can see an interesting fact. Although both of our examples are based on the same symmetry, a small variation can cause important differences in the phenomenology. Furthermore, it is unlikely that the modification of a model shall affect only one single observable. As we can see in the figures, although the second model allows us to achieve a larger $S_{\psi\phi}$, which is needed to solve the dimuon anomaly, this generates large deviations in $S_{\psi K_s}$, which is kept under much better control in the first model.

This is something to be expected of all Flavoured CMSSM models: as soon as one observable gets enhanced, one shall need to verify that all other important observables do not exceed their bounds. It would be desirable to follow patterns such as the one shown in these examples, where $S_{\psi\phi}$ is somewhat increased, and then ε_K and $S_{\psi K_s}$ receive very small contributions in the proper directions, such that their tension is cancelled.

4.3.2 EDMs and LFV

As in the previous CMSSM model with RH neutrinos, LFV processes can impose strong constraints on the parameter space of Flavoured CMSSM models. For the examples we have taken, it was shown in [34] that both neutralino and chargino loops contributed significantly to the decay, being

[11] Note that the LHCb collaboration has recently carried out a combined analysis of $B_s \to \psi\phi$ and $B_s \to \psi f_0(980)$ with 0.3 fb^{-1}. The central value agrees with the SM prediction, albeit with large errors, $2\beta^{\text{exp}}_s = 0.03 \pm 0.16 \pm 0.07$ [100].

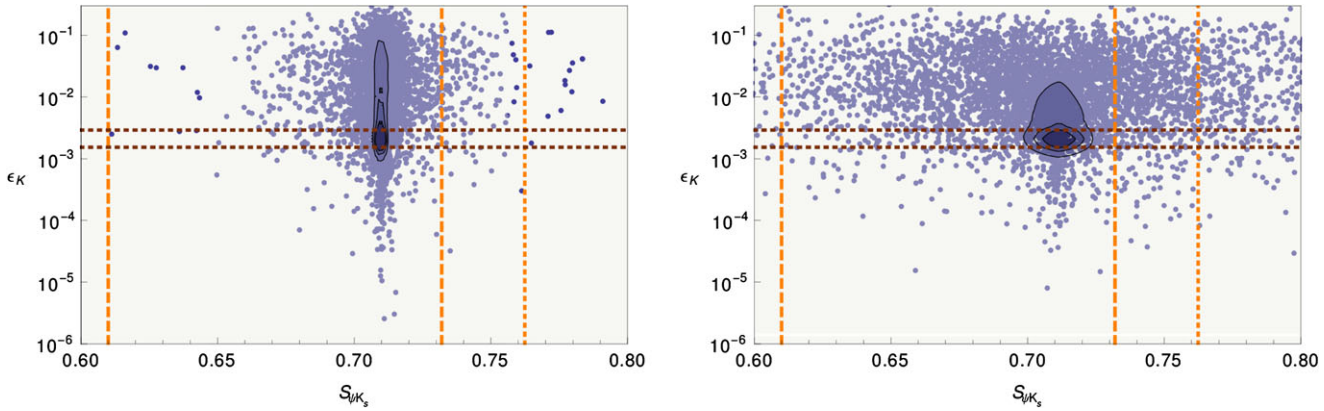

Fig. 9 Constraints due to $S_{\psi K_s}$ and ε_K in Model 1 (*left*) and Model 2 (*right*) from [35]. *Dotted* (*dashed*) *lines* correspond to 3σ (2σ) constraints. All points satisfy LFV constraints

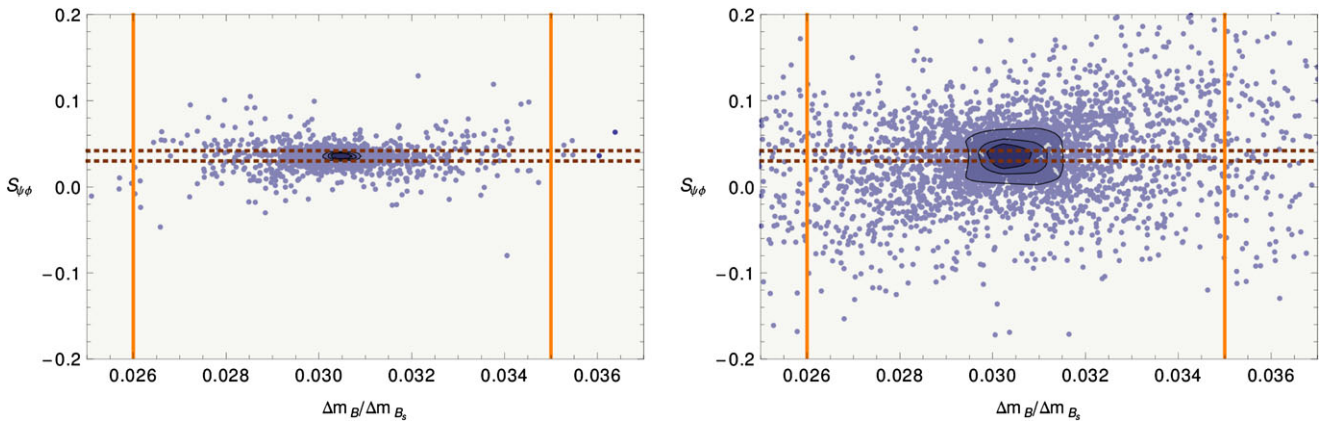

Fig. 10 Values of $S_{\psi\phi}$ and constraints due to $\Delta m_B/\Delta m_{B_s}$ in Model 1 (*left*) and Model 2 (*right*) from [35]. The *dashed* (*solid*) *lines* correspond to 2σ (1σ) constraints

the situation particularly restrictive when $A_0 \neq 0$ due to an enhancement in the neutralino contribution. In addition, if the EDMs are generated by flavour-dependent phases, one could expect interesting correlations to arise between them and flavour-violating processes.

We show correlations between observables of interest in Fig. 11. This time, when comparing both our examples, we do not find major differences between them, so we shall only show results for the first one. In all panels, points in pink give too large contributions to neutral meson processes, and are ruled out, whilst points in blue are allowed. Contours refer to the qualitative density of blue points. The solid lines give the current bounds for both processes, whilst the dashed line gives the future prospects.

On the left panel of Fig. 11, we show the predictions for $\mathrm{BR}(\mu \to e\gamma)$ vs. d_e. Apart from the current and future bounds, we also show in dotted lines the old MEGA bound for $\mu \to e\gamma$. We find that, in general, $\mu \to e\gamma$ and the neutral meson bounds, such as ε_K, work in opposite directions. Most points that satisfy the $\mu \to e\gamma$ bound are ruled out by the quark sector constraints, leaving only a relatively small number of points allowed. This is mainly due to the fact that ε_K prefers points with low m_0, which are in turn ruled out by the neutralino contribution to $\mu \to e\gamma$ whenever $|a_0| \gtrsim 1$. We find that the points not ruled out by the current MEG bound do not have a too large value for d_e. Furthermore, we can see that the future prospects for MEG, combined with our conservative expectation for d_e (based on [103–106]), can probe most of the still-allowed points in both models.

The central panel shows $\mathrm{BR}(\mu \to e\gamma)$ vs. $\mathrm{BR}(\tau \to \mu\gamma)$. We see that both processes are useful for probing the parameter space. However, we find that very few points surviving the MEG constraint are ruled out by the current $\tau \to \mu\gamma$ bound. In addition, when looking at the future prospects, we can see that $\tau \to \mu\gamma$ is not as strong as $\mu \to e\gamma$ or d_e in constraining the model.

Finally, the right panel shows the predictions for d_n in both the CQ and QP models. In this panel, the pink dots also indicate points ruled out by LFV processes. Notice that, as we are comparing two neutron models, the only points effectively ruled out by d_n lie on the upper right square limited by the solid lines. We find that, after applying all bounds,

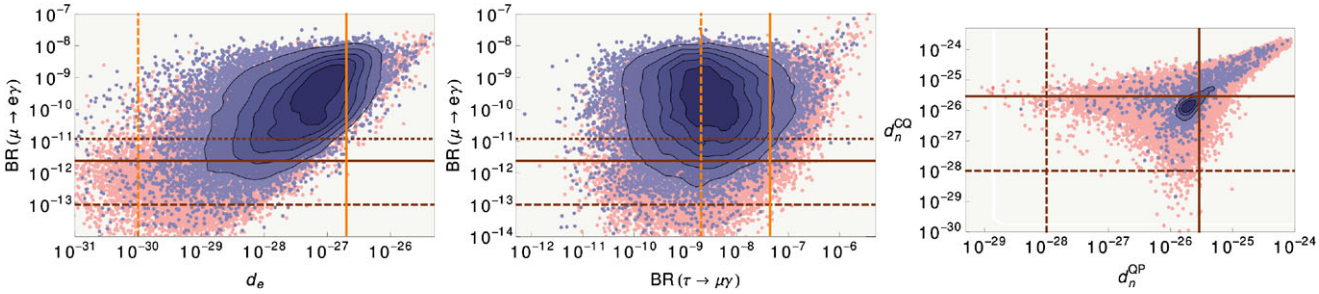

Fig. 11 Several prediction for LFV and EDMs, for the first example from [35]. On the *left panel*, we have $\mathrm{BR}(\mu \to e\gamma)$ vs. d_e, on the *central panel* we show $\mathrm{BR}(\mu \to e\gamma)$ vs. $\mathrm{BR}(\tau \to \mu\gamma)$ and on the *right* we compare d_n^{CQ} and d_n^{QP}. On all plots, *solid lines* indicate current bounds, whilst *dashed lines* indicate prospects in future experiments. For $\mathrm{BR}(\mu \to e\gamma)$, the *dotted line* shows the old MEGA bound. *Pink points* are ruled out by meson constraints

not many points are left. In addition, a future improvement in the measurement of d_n [107–110] would be able to probe the square limited by the dashed lines, i.e. all but the most fine-tuned points. Thus, if neutron EDM models prove to be consistent, we find that d_n is the observable most sensitive to the predictions of these example models.

4.3.3 Allowed parameter space

To summarise, we find that a Flavoured CMSSM can be expected to saturate the neutral meson bounds, particularly in the CP violating sectors. Furthermore, the $\mu \to e\gamma$ branching ratio can rule out a sizeable amount of points that do satisfy the neutral meson bounds, providing a complementary constraint. Thus, although flavoured models such as those provided in the examples are not ruled out and can still provide interesting predictions, the allowed parameter space should be expected to be heavily constrained.

In Fig. 12 we show the available parameter space for our example models. In the top row we show the m_0–$M_{1/2}$ plane, where we see that usually small values of m_0 are preferred, which due mainly to the ε_K constraint. The preference for small m_0 can be understood through the additional RG suppression factor $m_0^2/(m_0^2 + 6M_{1/2}^2)$, which keeps ε_K under control. For the first example we see an additional higher-density area at larger m_0, which we interpret as being due to interference between $(\delta_{12}^d)_{LL}(\delta_{12}^d)_{RR}$ and $(\delta_{12}^d)_{RR}^2$ insertions, as explained in [37]. Note, however, that for both models it is still possible to reach large values of m_0, even though they are not common.

The central row shows the preference for $a_0 \to 0$ in the m_0–a_0 plane. This is mainly due to the sizeable additional neutralino contribution that saturates $\mu \to e\gamma$. It must be noted, however, that as each term of the trilinears is multiplied by an arbitrary $\mathcal{O}(1)$, the values of a_0 shown in this plot just indicate an approximate number around which the trilinears shall vary. Thus, they should not be compared to the respective plots for the CMSSM, unless $a_0 = 0$.

The bottom row shows the allowed points in the m_0–$\tan\beta$ plane. We find that, generally, small values of $\tan\beta$ shall be preferred, although large values can still be found. We see that the first model allows larger values of $\tan\beta$ than the second, which is mainly due to the fact that the latter includes a $\tan\beta$ enhancement to $(\delta_{RR}^{d,e})_{i3}$ insertions, which can exceed the neutral meson bounds.

A valid question is whether these models survive if we demand all observables to satisfy the 2σ constraints, as we did in the CMSSM. The answer is affirmative, although the strong bounds considerably reduce the amount of points. The main result is that only those points with small m_0, moderate $\tan\beta$ and small a_0 (typically, $m_0 \lesssim 500$ GeV, $\tan\beta \lesssim 20$ and $|a_0| \lesssim 1$) manage to survive. In particular, it is remarkable that, despite the stringent MEG and ε_K constraints, they can still provide a sizeable contribution to a_μ, such that the tension with the experiments can be lowered below the 2σ level.

To conclude, even though we have restricted our attention to only two models of our interest, we can say that for a Flavoured CMSSM we can expect an important interplay between collider and flavour observables. In particular, we confirm our earlier claim of [34], where we estimated that this combination of data would be able to fully probe the $SU(3)$ models if SUSY was light enough. Thus, although strongly constrained, these examples can still fit within an early SUSY discovery scenario, and give interesting and verifiable predictions for low-energy experiments.

4.4 LHC observables

In the previous sections, we have analysed possible signals in flavour observables in the region of the MSSM parameter space that would be observable as an excess in the jets plus missing energy channel at the LHC with 5 fb^{-1}. In this section we provide examples of the expected signals at LHC for three benchmark points in the "observable" region.

As explained in Sect. 4.1, this observable region was estimated using the results of [10]. Following that analysis, we

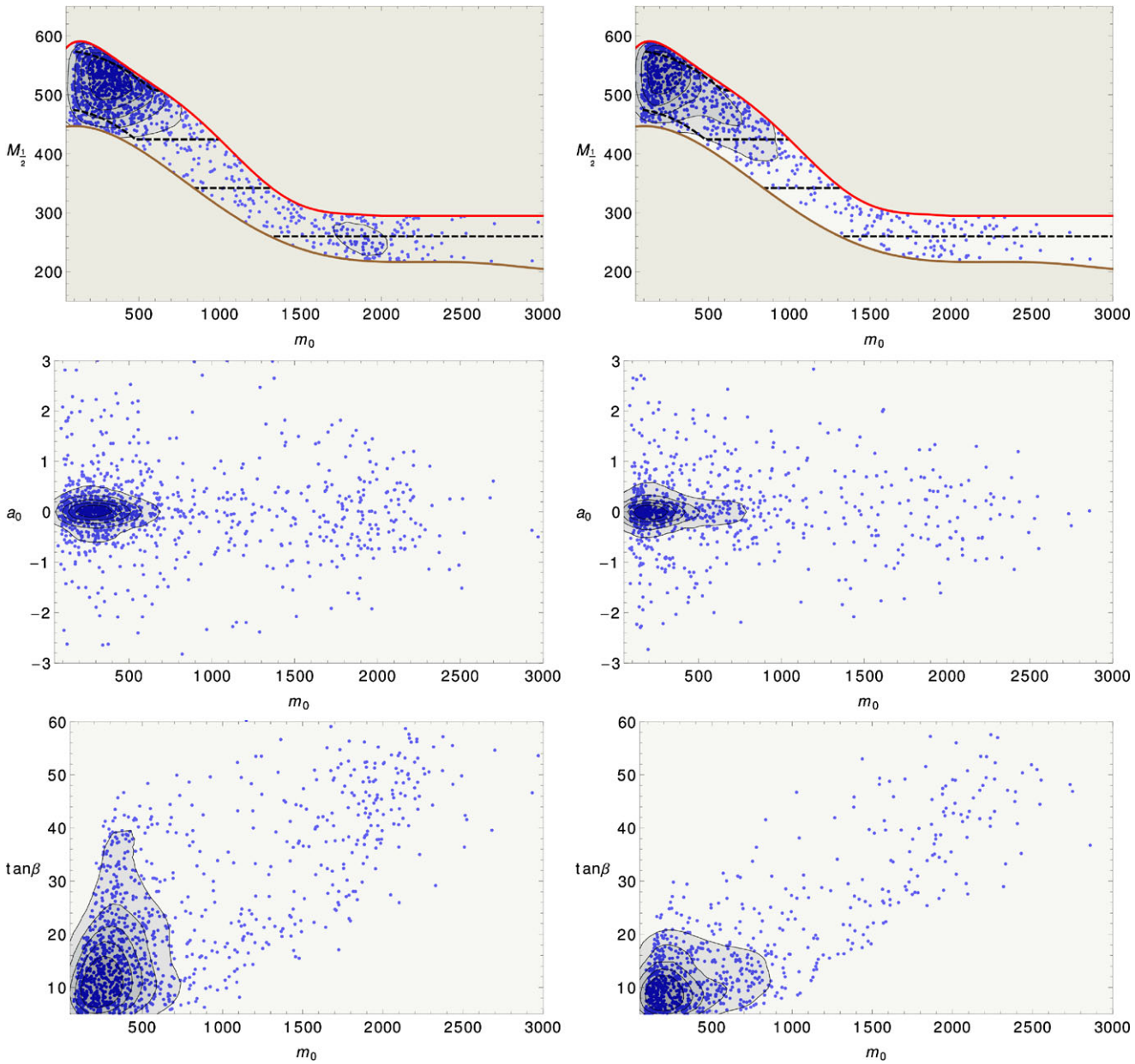

Fig. 12 Area in the m_0–$M_{1/2}$ (*top*), m_0–a_0 (*centre*) and m_0–$\tan\beta$ (*bottom*) planes for Model 1 (*left*) and Model 2 (*right*), including CPV bounds in meson mixing and LFV constraints

define a point in the MSSM parameter space to be observable when the expected number of signal events S after the cuts are,

$$S \geq \max\left[5\sqrt{B}, 5, 0.2\ B\right], \tag{23}$$

where B is the number of background events after the cuts. The set of cuts is optimised for each points using a grid of cuts in different variables to maximise $S/\sqrt{S+B}$ [10]. The cuts we use in our optimisation procedure are the missing transverse energy, $\not{E}_T$, number of jets, n(jets), number of b-jets, $n(b)$, transverse energy of the leading jet, $E_T(j_1)$ and transverse energy of the second jet, $E_T(j_2)$.

We select three benchmark points in the CMSSM parameter space (in the Seesaw, or Flavoured CMSSM, the LHC signal would be practically identical):

1. Benchmark A: $m_0 = 1330$ GeV, $m_{1/2} = 270$ GeV, $\tan\beta = 55$, $A_0 = 1830$ GeV. $\Rightarrow m_{\tilde{g}} = 712.6$ GeV, $m_{\tilde{q}_1} \simeq 1430$ GeV.
2. Benchmark B: $m_0 = 670$ GeV, $m_{1/2} = 385$ GeV, $\tan\beta = 22$, $A_0 = 1210$ GeV. $\Rightarrow m_{\tilde{g}} = 943.6$ GeV, $m_{\tilde{q}_1} \simeq 1055$ GeV.
3. Benchmark C: $m_0 = 170$ GeV, $m_{1/2} = 535$ GeV, $\tan\beta = 14$, $A_0 = -510$ GeV. $\Rightarrow m_{\tilde{g}} = 1235.5$ GeV, $m_{\tilde{q}_1} \simeq 1140$ GeV.

As we can see, Benchmark A corresponds to a relatively light gluino that whilst B and C correspond to progressively larger gluino masses. Squarks of the first generation are in all three benchmarks points heavier than 1 TeV, and in Benchmark A $m_{\tilde{q}_1} \sim 1.4$ TeV. Furthermore, only Benchmark C has squarks lighter than the gluino. These features determine the observable signal in the three different benchmark points.

We simulate the signal and background for these points using MadGraph [111] and PYTHIA [112] and the detector effects with PGS [113]. The simulated signal and background corresponds to a full 5 fb^{-1} simulation. In this framework, we choose, for each point, the set of cuts on $\not{E}_T$, $n(\text{jets})$, $n(b)$, $E_T(j_1)$ and $E_T(j_2)$, (making a grid of the possible values of the cuts as in [10]) that maximise the significance $S/\sqrt{S+B}$. Using this set of constraints, we are not making any requirement on the total energy, M_{eff}, of the event. In a second round, we use the minimum value of M_{eff} that we obtain for signal and background in the first round to set a new cut on M_{eff} and choose again the values of the aforementioned cuts that maximise the significance, taking now into account the minimum value of M_{eff}. Notice that adding this new cut on M_{eff}, would have no effect on the points selected by the previous set of constraints, but now, we are scanning again the constraints above in the subset of points with a minimum value of M_{eff} and choosing a new set of cuts that maximise $S/\sqrt{S+B}$. The final result of the number of S, B, significance and the set of applied cuts for each point are the following:

1. Cuts point A: $\not{E}_T \geq 200$ GeV, $n(\text{jets}) \geq 8$, $n(b) = 0$, $E_T(j_1) \geq 100$ GeV, $E_T(j_2) \geq 80$ GeV and $M_{\text{eff}} \geq 800$ GeV. $\Rightarrow S = 92$, $B = 247$, Signif. $= 5.0$
2. Cuts point B: $\not{E}_T \geq 300$ GeV, $n(\text{jets}) \geq 8$, $n(b) = 0$, $E_T(j_1) \geq 50$ GeV, $E_T(j_2) \geq 50$ GeV and $M_{\text{eff}} \geq 900$ GeV. $\Rightarrow S = 76$, $B = 60$, Signif. $= 6.5$
3. Cuts point C: $\not{E}_T \geq 600$ GeV, $n(\text{jets}) \geq 2$, $n(b) = 0$, $E_T(j_1) \geq 300$ GeV, $E_T(j_2) \geq 110$ GeV and $M_{\text{eff}} \geq 1400$ GeV. $\Rightarrow S = 37$, $B = 39$, Signif. $= 4.2$

In Figs. 13, 14 and 15, we plot the distribution of background and signal events in M_{eff}, $\not{E}_T$ and $n(\text{jets})$ for all three points after applying the corresponding cuts. Although the

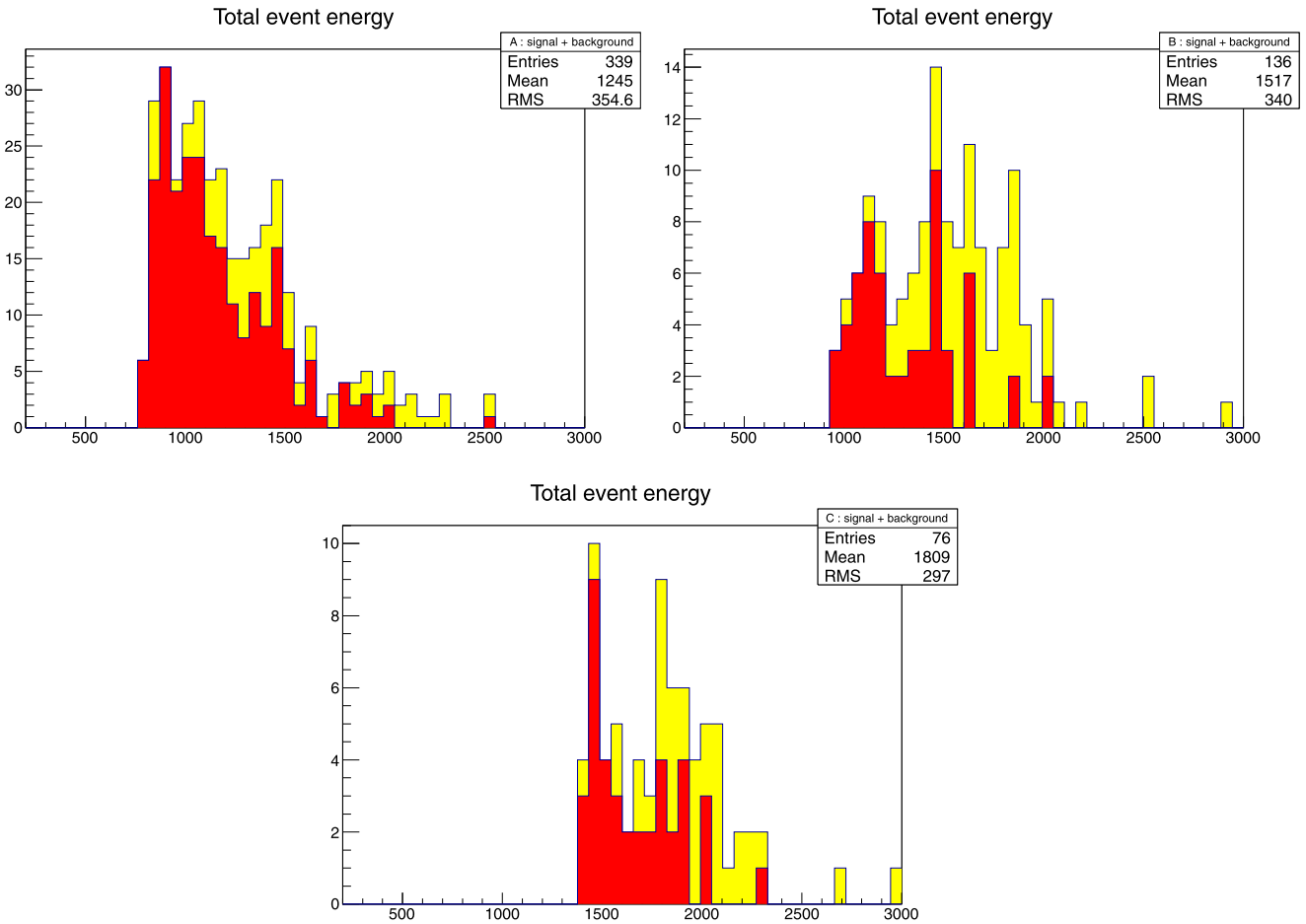

Fig. 13 (Color online) Distribution of background and signal events as a function of M_{eff} after the corresponding cuts for benchmark points A (*left*), B (*right*) and C (*centre*). The background events are plotted in *red* and the signal + background events in *yellow*

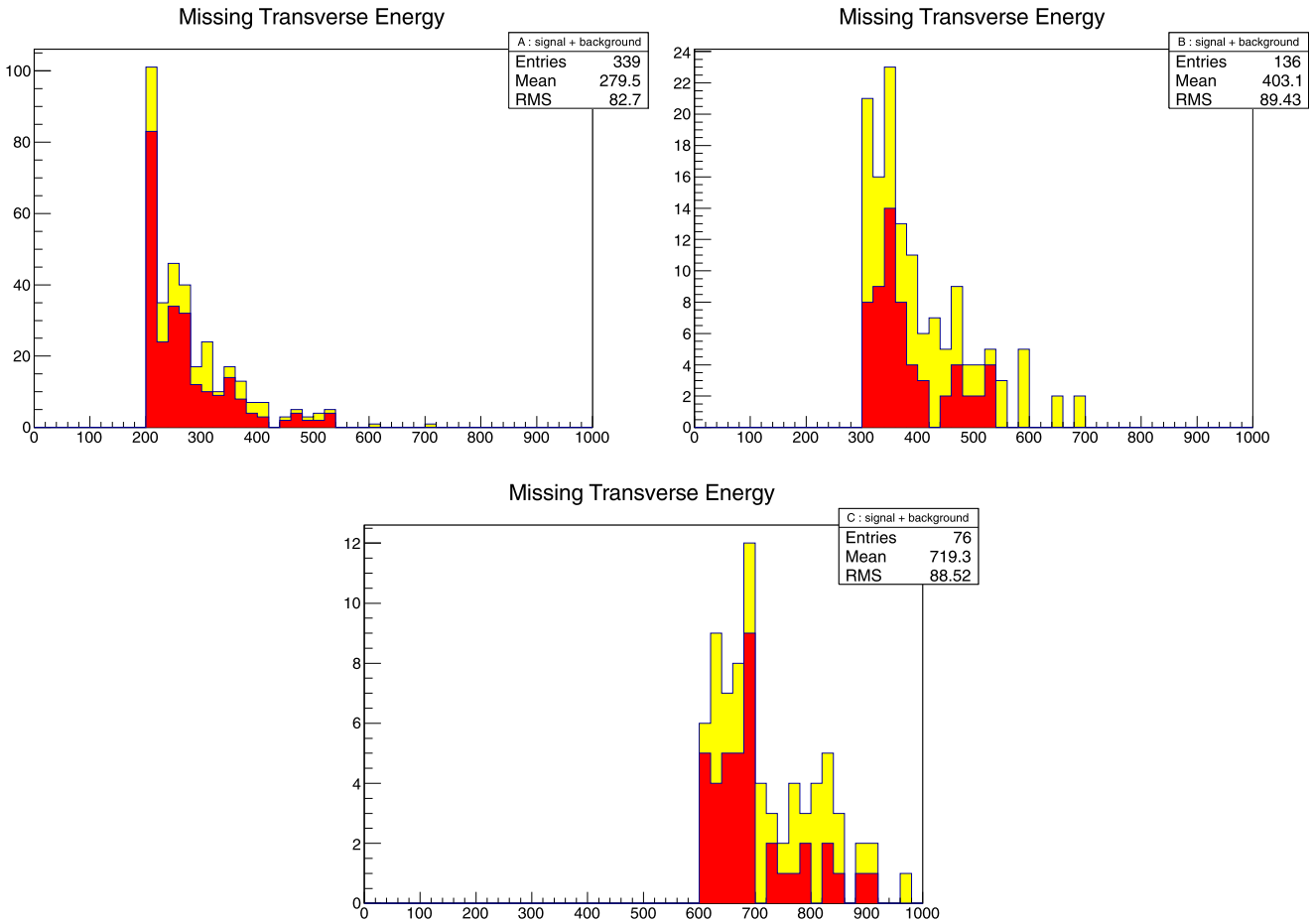

Fig. 14 (Color online) Distribution of events as a function of $\not\!\!E_T$ after the corresponding cuts for benchmark points A (*left*), B (*right*) and C (*centre*). The background events are plotted in *red* and the signal + background in *yellow*

statistics is still limited for the three points, these figures give an idea of the expected signal at LHC with 5 fb^{-1}.

From the analysis of M_{eff} in Fig. 13, we see that in points A and B signal plus background have a broad distribution of events centred roughly at $M_{\text{eff}} \sim 1300$ GeV and $M_{\text{eff}} \sim 1500$ GeV respectively and for point C the events are centred around $M_{\text{eff}} \sim 2000$ GeV. However, it is hard to make a more precise statement on the value of M_{eff} due to the limited statistics. In fact, the excess of events above the expected background is of order 100 events for points A and B and of order 30 for point C. For these signal events, points A and B are hard to distinguish in this plot. From Figs. 14 and 15, we see that points A and B are still very similar and it is difficult to distinguish them with these observables and limited statistics. In Fig. 15, we can see that the jet number is very different for point C and the rest. In points A and B, we have on average a large number of jets, whilst point C has a smaller number of jets. Although this is partly an effect of the imposed cut on number of jets ($n(\text{jets}) \geq 8$ for A and B and $n(\text{jets}) \geq 2$ for C), it is clear that we have events in A and B with a much larger number of jets than for point C. This is a clue on the nature of the coloured sparticles produced in the collision. We must take into account that the main SUSY production channels are either two gluinos, two first-generation squarks or a gluino plus a first generation squark. Clearly, if the event consists of the production of a pair of gluinos, we will have on average two additional jets with respect to the production of two squarks and analogously for the case of production of a squark and a gluino. Therefore, from this, we would expect that points A and B correspond mainly to the production of gluino pairs whilst point C, where there is a significant excess in two- and three-jet events, this excess must correspond to the production of a pair of first generation squarks (cf. the SUSY production cross sections for our three benchmark points, as computed by PROSPINO 2.0 [45], in Table 6). Given that this two- and three-jet excess is a significant part ($\sim 1/3$) of total excess of events, we would conclude that the production of first generation squarks in this point is important and the masses of first generation squarks are probably lighter or at least of the order of the gluino mass. Although it is difficult to make quantitative statements, using the approximate relation

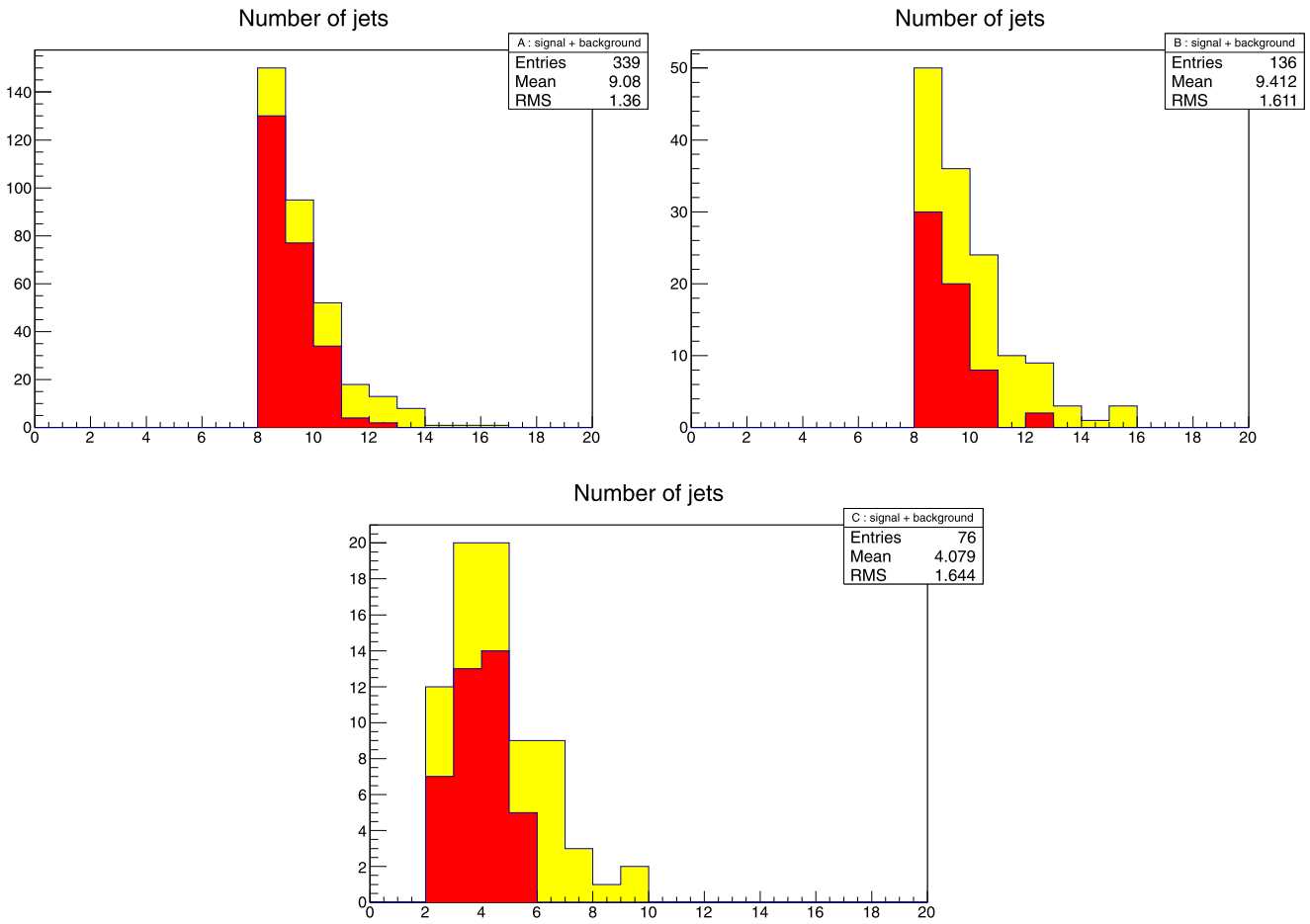

Fig. 15 (Color online) Distribution of events as a function of n(jets) after the corresponding cuts for benchmark points A (*left*), B (*right*) and C (*centre*). The background events are plotted in *red* and the signal + background in *yellow*

Table 6 SUSY production cross section (expressed in fb) for different channels

	Point A	Point B	Point C
$\sigma_{\tilde{g}\tilde{g}}$	155	10	0.5
$\sigma_{\tilde{q}\tilde{q}}$	1.5	28	14
$\sigma_{\tilde{q}\tilde{q}^*}$	0.1	4	2
$\sigma_{\tilde{q}\tilde{g}}$	33	43	7.5
$\sigma_{\tilde{t}\tilde{t}^*}$	0.003	0.1	0.05
$\sigma_{\tilde{b}\tilde{b}^*}$	0.003	0.1	0.05
σ_{tot}	190	85	24

$M_{\text{eff}} \sim 1.6\, M_{\text{SUSY}}$, with M_{SUSY} the lightest coloured particle mass, $M_{\text{SUSY}} = \min(m_{\tilde{g}}, m_{\tilde{q}_1})$, we would roughly expect that $m_{\tilde{g}} \sim 900$ GeV for points A and B and $m_{\tilde{q}_1} \sim 1250$ GeV for point C. Finally, the analysis of the missing E_T in Fig. 14 provides also some very interesting information on the mass splitting from the initially produced coloured sparticle and the LSP. The largest possible missing energy corresponds to the two LSPs carrying away, each of them, one half of the mass splitting between the initially produced sparticle and the LSP. Therefore, for the points A and B, where the maximum missing E_T is of order of 700 GeV, we would conclude that the mass difference between the gluino and the lightest neutralino is 700 GeV, and thus we could roughly estimate $m_{\tilde{\chi}_1^0} \sim 240$ GeV. Similarly, for point C, where the maximum missing E_T is 900 GeV, we would estimate a lightest neutralino mass of $m_{\tilde{\chi}_1^0} \sim 350$ GeV.

Even though we can obtain much information from our analysis, we see that it is very difficult to distinguish points A and B with collider observables at 5 fb^{-1}. At this point, one can turn to flavour for more information. For instance, from the previous sections, we know that the measurement of BR($B_s \to \mu^+\mu^-$) can separate regions in the parameter space. In fact, a 2 fb^{-1} search at LHCb would show a 3σ evidence for this decay in point A, whilst leaving point B and C consistent with the SM expectations. Thus, $B_s \to \mu^+\mu^-$ can favour one region of the parameter space over another in light of collider data.

Moreover, flavour provides more tools than just point differentiation. The flavour phenomenology can be reintro-

Table 7 Central values for some flavour observables in each benchmark point. All points satisfy 2σ constraints once experimental and theoretical errors are included

Benchmark	BR($b \to s\gamma$)	δa_μ	BR($B_d \to \mu^+\mu^-$)	BR($B_s \to \mu^+\mu^-$)	$R(B^+ \to \tau_v^+)$
A	3.00×10^{-4}	1.06×10^{-9}	2.01×10^{-10}	6.36×10^{-9}	0.60
B	2.89×10^{-4}	1.05×10^{-9}	1.20×10^{-10}	3.80×10^{-9}	0.97
C	2.92×10^{-4}	1.07×10^{-9}	1.21×10^{-10}	3.81×10^{-9}	0.99

duced to the collider observations as a way of roughly testing the coherence of our main assumption, namely, that the SUSY spectrum is close to that described by the CMSSM. Thus, it is possible to provide some "flavour feedback" to colliders.

For instance, requiring the 2σ flavour constraints on $b \to s\gamma$ and $(g-2)_\mu$ to be satisfied (which is true for all benchmark points, as seen in Table 7), evidence for $B_s \to \mu^+\mu^-$ leads us to favour relatively large values of $\tan\beta$, A_0 and m_0, as was shown in Fig. 5. Combining this with the rough $M_{\rm eff}$ contours, one can expect to obtain some information on $M_{1/2}$. For instance, in point A, as the large m_0 leads to large squark masses, we would require a light gluino to be responsible for the $M_{\rm eff}$ measurement, as was made evident from our collider analysis. This gives us direct information on the value of $M_{1/2}$.

Once this information is obtained, one can then check the consistency with rest of the collider information. As we have mentioned, the fact that the gluino is the dominant source of the excess in jets has a direct repercussion on the number of jets we should observe, and this should be consistent with both $M_{\rm eff}$ and flavour data. Also, the endpoint of the $\not{E}_T$ distribution would give us an idea of the splitting between this gluino and the LSP, which tests directly the assumption of gaugino universality.

On the other hand, we could have no evidence whatsoever for $B_s \to \mu^+\mu^-$. In this case, inspection of Fig. 5 does not allow us to make such strong statements as those done for point A. We find that larger values of $M_{1/2}$ are favoured, but we cannot expect to be able to reach a conclusion regarding m_0, unless we are in a very special scenario with very large or very low $M_{\rm eff}$.

Still, even if $B_s \to \mu^+\mu^-$ is not observed, the interplay with $b \to s\gamma$ and $(g-2)_\mu$ does give information about $\tan\beta$ and A_0. For example, if $M_{\rm eff}$ is low enough, one can determine the sign of A_0, as well as give upper and lower bounds on $\tan\beta$. This is the case in point B. For too high $M_{\rm eff}$, one only obtains an upper bound on m_0 due the LHC reach, and from this it is possible to establish an upper bound on $\tan\beta$. Nevertheless, it shall be unfeasible to carry out any self-consistency tests with only this amount of information.

Moreover, notice that the different models considered in this paper, the CMSSM, the Seesaw CMSSM or the Flavoured CMSSM, have a very similar spectrum and would give identical information in collider observables. Flavour here becomes again useful, as one can take this information and go to indirect searches, mainly $\mu \to e\gamma$, neutral meson mixing and electric dipole moments. Clearly, if a positive signal is found in any of these indirect observables, the CMSSM has to be abandoned and we have to increase the number of parameters in the model.

5 Conclusions

We have discussed the interplay between LHC and flavour and CP violation experiments in testing supersymmetric models. Under the assumption that a hint for SUSY particles will be indeed found at LHC7 (after analysing 5 fb^{-1} of data), and taking into account the exclusion bounds already provided by ATLAS and CMS, we have studied the consequent SUSY predictions for flavour and CPV observables. This analysis has been performed for a set of phenomenologically motivated SUSY models, namely the CMSSM, a SUSY seesaw and a Flavoured CMSSM, i.e. an extension of the CMSSM with non-trivial flavour structures controlled by the same dynamics responsible for the SM fermion masses and mixing. In particular, we focussed on the capability of flavour experiments to discriminate among different models and to constrain or give information on the parameters of a given model. The outcome of our study can be summarised as follows.

- As expected, LHC experiments and flavour observables are complementary in probing the SUSY parameter space. In particular, the imposition of flavour constraints (especially BR($b \to s\gamma$) and $(g-2)_\mu$) can give information on the SUSY parameters that are not directly constrained by jets plus $\not{E}_T$ searches at LHC (such as A_0 and $\tan\beta$).
- Positive or negative results of $B_s \to \mu^+\mu^-$ searches at LHCb and CMS can further disentangle different regimes of the parameters, in some cases selecting very restricted allowed values. In general $B_s \to \mu^+\mu^-$ seems to be a crucial test for SUSY models, in case non-standard signals are observed at LHC.
- The interplay of LHC and the MEG experiment will be crucial to probe SUSY seesaw scenarios, providing indirect information on the neutrino Yukawa mixing and/or

the RH neutrino mass scale. In particular large-mixing, large-Yukawa scenarios are already ruled out by the recent MEG limits on BR($\mu \to e\gamma$). Neutrino oscillation and $(g-2)_\mu$ experiments can further increase our capability to access the seesaw parameters and thus to test indirectly very high-energy scales.

– In some simple seesaw scenarios, the preferred range for U_{e3} recently reported by T2K implies small rates for the $\tau \to \mu\gamma$ decay. Therefore, such scenarios can be excluded by evidence for $\tau \to \mu\gamma$ at the Super B factories.
– The Flavoured CMSSM we considered is still a viable model for addressing the SM and the SUSY flavour problems at the same time. Interesting correlations among different observables (such as ε_K and $\mu \to e\gamma$) tend to restrict the allowed parameter space also in this case. LFV and EDM experiments will completely test the model at least within the region accessible at LHC7 with 5 fb^{-1}, providing an important cross-check of the LHC findings. On the other hand, a large phase of the B_s mixing would disfavour this kind of scenario.
– The observability at LHC7 of the parameter space region we studied and the features of the signals have been checked for three benchmark points in Sect. 4.4 by means of numerical simulations. We have shown that set-ups which provide similar signatures at LHC7 can be actually distinguished by means of flavour observables (especially $B_s \to \mu^+\mu^-$) and the interplay between collider and flavour signatures can provide useful information in the attempt of determining the fundamental parameters of the model.

As a final conclusion, although CMSSM-like models are currently considered somewhat disfavoured in light of the latest ATLAS and CMS results, we find that they can still provide very interesting phenomenology and correlations in both the collider and flavour sectors. The current run of the LHC is still exciting for SUSY, and it may be possible to find surprises just around the corner.

Acknowledgements We thank Massimo Passera and Jonas Lindert for useful discussions, Werner Porod for the assistance provided with SPheno, and Joachim Brod for pointing out a mistake in Table 5. L.C., J.J.P., A.M. and O.V. thank the Galileo Galilei Institute for Theoretical Physics for the hospitality and the INFN for partial support during the workshop that gave birth to this work. L.C., J.J.P., R.N.H. and O.V. thank the Università di Padova for the hospitality and support provided during their visit. L.C. and J.J.P. are grateful to the Universitat de València for hospitality and financial support during several stages of this work. J.J.P. would also like to thank the Max-Planck-Institut für Physik for the hospitality and support provided during his visit. A.M. acknowledges the contribution of the CARIPARO Excellence Project "LHC and Cosmology". We acknowledge further support from the MICINN-INFN agreements ACI2009-1049 and INFN2008-016. O.V. and R.N.H. acknowledge partial support by MEC and FEDER (EC), Grants No. FPA2008-02878 and FPA2011-23596 and by the Generalitat Valenciana under the grant PROMETEO/2008/004.

References

1. S. Chatrchyan et al. (CMS Collaboration), arXiv:1109.2352 [hep-ex]
2. G. Aad et al. (ATLAS Collaboration), arXiv:1109.6572 [hep-ex]
3. A. Strumia, J. High Energy Phys. **1104**, 073 (2011). arXiv:1101.2195 [hep-ph]
4. P. Minkowski, Phys. Lett. B **67**, 421 (1977)
5. M. Gell-Mann, P. Ramond, R. Slansky, in *Supergravity*, ed. by P. van Niewenhuizen, D. Freedman (North-Holland, Amsterdam, 1979), p. 315
6. T. Yanagida, in *Proceedings of the Workshop on the Unified Theory and the Baryon Number in the Universe*, ed. by O. Sawada, A. Sugamoto. KEK Report No. 79-18, Tsukuba (1979), p. 95
7. R.N. Mohapatra, G. Senjanović, Phys. Rev. Lett. **44**, 912 (1980)
8. C.D. Froggatt, H.B. Nielsen, Nucl. Phys. B **147**, 277 (1979)
9. M. Raidal, A. van der Schaaf, I. Bigi, M.L. Mangano, Y.K. Semertzidis, S. Abel, S. Albino, S. Antusch et al., Eur. Phys. J. C **57**, 13–182 (2008). arXiv:0801.1826 [hep-ph]
10. H. Baer, V. Barger, A. Lessa, X. Tata, J. High Energy Phys. **1006**, 102 (2010). arXiv:1004.3594 [hep-ph]
11. I. Hinchliffe, F.E. Paige, M.D. Shapiro, J. Soderqvist, W. Yao, Phys. Rev. D **55**, 5520–5540 (1997). arXiv:hep-ph/9610544
12. D.R. Tovey, Phys. Lett. B **498**, 1–10 (2001). arXiv:hep-ph/0006276
13. G. D'Ambrosio, G.F. Giudice, G. Isidori, A. Strumia, Nucl. Phys. B **645**, 155–187 (2002). arXiv:hep-ph/0207036
14. S. Profumo, Phys. Rev. D **84**, 015008 (2011). arXiv:1105.5162 [hep-ph]
15. O. Buchmueller, R. Cavanaugh, D. Colling, A. De Roeck, M.J. Dolan, J.R. Ellis, H. Flacher, S. Heinemeyer et al., Eur. Phys. J. C **71**, 1722 (2011). arXiv:1106.2529 [hep-ph]
16. L. Calibbi, Y. Mambrini, S.K. Vempati, J. High Energy Phys. **0709**, 081 (2007). arXiv:0704.3518 [hep-ph]
17. V. Barger, D. Marfatia, A. Mustafayev, Phys. Lett. B **665**, 242–251 (2008). arXiv:0804.3601 [hep-ph]
18. F. Borzumati, A. Masiero, Phys. Rev. Lett. **57**, 961 (1986)
19. J. Hisano, T. Moroi, K. Tobe, M. Yamaguchi, Phys. Rev. D **53**, 2442 (1996). arXiv:hep-ph/9510309
20. J. Hisano, M. Nagai, P. Paradisi, Y. Shimizu, J. High Energy Phys. **0912**, 030 (2009). arXiv:0904.2080 [hep-ph]
21. A. Masiero, S.K. Vempati, O. Vives, Nucl. Phys. B **649**, 189 (2003). arXiv:hep-ph/0209303
22. L. Calibbi, A. Faccia, A. Masiero, S.K. Vempati, Phys. Rev. D **74**, 116002 (2006). arXiv:hep-ph/0605139
23. J.A. Casas, A. Ibarra, Nucl. Phys. B **618**, 171–204 (2001). arXiv:hep-ph/0103065
24. K. Abe et al. (T2K Collaboration), Phys. Rev. Lett. **107**, 041801 (2011). arXiv:1106.2822 [hep-ex]
25. Y. Nomura, M. Papucci, D. Stolarski, Phys. Rev. D **77**, 075006 (2008). arXiv:0712.2074 [hep-ph]
26. M. Leurer, Y. Nir, N. Seiberg, Nucl. Phys. B **398**, 319 (1993). arXiv:hep-ph/9212278
27. R. Barbieri, G.R. Dvali, L.J. Hall, Phys. Lett. B **377**, 76 (1996). arXiv:hep-ph/9512388
28. G. Altarelli, F. Feruglio, Nucl. Phys. B **720**, 64 (2005). arXiv:hep-ph/0504165
29. S.F. King, G.G. Ross, Phys. Lett. B **520**, 243 (2001). arXiv:hep-ph/0108112
30. Z. Lalak, S. Pokorski, G.G. Ross, J. High Energy Phys. **1008**, 129 (2010). arXiv:1006.2375 [hep-ph]
31. S.F. King, G.G. Ross, Phys. Lett. B **574**, 239 (2003). arXiv:hep-ph/0307190
32. R.G. Roberts, A. Romanino, G.G. Ross, L. Velasco-Sevilla, Nucl. Phys. B **615**, 358 (2001). arXiv:hep-ph/0104088
33. G.G. Ross, L. Velasco-Sevilla, O. Vives, Nucl. Phys. B **692**, 50 (2004). arXiv:hep-ph/0401064

34. L. Calibbi, J. Jones-Perez, O. Vives, Phys. Rev. D **78**, 075007 (2008). arXiv:0804.4620 [hep-ph]
35. L. Calibbi, J. Jones-Perez, A. Masiero, J.H. Park, W. Porod, O. Vives, Nucl. Phys. B **831**, 26 (2010). arXiv:0907.4069 [hep-ph]
36. W. Altmannshofer, A.J. Buras, S. Gori, P. Paradisi, D.M. Straub, Nucl. Phys. B **830**, 17 (2010). arXiv:0909.1333 [hep-ph]
37. J. Jones-Perez, Flavour and CP violation phenomenology with supersymmetric flavour symmetries. PhD Thesis, 2010
38. M. Ciuchini, G. D'Agostini, E. Franco, V. Lubicz, G. Martinelli, F. Parodi, P. Roudeau, A. Stocchi, J. High Energy Phys. **0107**, 013 (2001). hep-ph/0012308, http://www.utfit.org/
39. W. Porod, Comput. Phys. Commun. **153**, 275 (2003). arXiv:hep-ph/0301101
40. W. Porod, F. Staub, arXiv:1104.1573 [hep-ph]
41. B.C. Allanach, T.J. Khoo, C.G. Lester, S.L. Williams, J. High Energy Phys. **1106**, 035 (2011). arXiv:1103.0969 [hep-ph]
42. S. Akula, N. Chen, D. Feldman, M. Liu, Z. Liu, P. Nath, G. Peim, Phys. Lett. B **699**, 377 (2011). arXiv:1103.1197 [hep-ph]
43. O. Buchmueller, R. Cavanaugh, A. De Roeck, M.J. Dolan, J.R. Ellis, H. Flacher, S. Heinemeyer, G. Isidori et al., arXiv:1110.3568 [hep-ph]
44. A. Fowlie, A. Kalinowski, M. Kazana, L. Roszkowski, Y.L.S. Tsai, arXiv:1111.6098 [hep-ph]
45. W. Beenakker, R. Hopker, M. Spira, arXiv:hep-ph/9611232
46. CMS and LHCb Collaborations, CMS-PAS-BPH-11-019, LHCb-CONF-2011-047, CERN-LHCb-CONF-2011-047
47. D. Asner et al. (Heavy Flavor Averaging Group Collaboration), arXiv:1010.1589 [hep-ex]. http://www.slac.stanford.edu/xorg/hfag/
48. J. Adam et al. (MEG Collaboration), arXiv:1107.5547 [hep-ex]
49. B. Aubert et al. (BABAR Collaboration), Phys. Rev. Lett. **104**, 021802 (2010). arXiv:0908.2381 [hep-ex]
50. V. Tisserand, arXiv:0905.1572 [hep-ph]
51. B. Aubert et al. (BABAR Collaboration), Phys. Rev. Lett. **104**, 021802 (2010). arXiv:0908.2381 [hep-ex]
52. K. Hagiwara, R. Liao, A.D. Martin, D. Nomura, T. Teubner, J. Phys. G **38**, 085003 (2011). arXiv:1105.3149 [hep-ph]
53. K. Nakamura et al. (Particle Data Group Collaboration), J. Phys. G **37**, 075021 (2010). http://pdg.lbl.gov/
54. (LHCb Collaboration), LHCb-CONF-2011-049
55. V.M. Abazov et al. (D0 Collaboration), arXiv:1109.3166 [hep-ex]
56. A. Abulencia et al. (CDF Collaboration), Phys. Rev. Lett. **97**, 242003 (2006). hep-ex/0609040
57. C.A. Baker et al., Phys. Rev. Lett. **97**, 131801 (2006). arXiv:hep-ex/0602020
58. B.C. Regan, E.D. Commins, C.J. Schmidt, D. DeMille, Phys. Rev. Lett. **88**, 071805 (2002)
59. E. Lunghi, J. Matias, J. High Energy Phys. **0704**, 058 (2007). arXiv:hep-ph/0612166
60. T. Moroi, Phys. Rev. D **53**, 6565 (1996) [Erratum-ibid. D **56**, 4424 (1997)]. arXiv:hep-ph/9512396
61. M. Passera, W.J. Marciano, A. Sirlin, Phys. Rev. D **78**, 013009 (2008). arXiv:0804.1142 [hep-ph]
62. V. Gibson (LHCb Collaboration), LHCb-TALK-2011-092
63. A.G. Akeroyd, F. Mahmoudi, D.M. Santos, arXiv:1108.3018 [hep-ph]
64. T. Aaltonen et al. (CDF Collaboration), Phys. Rev. Lett. **107**, 191801 (2011). arXiv:1107.2304 [hep-ex]
65. W.C. Griffith, M.D. Swallows, T.H. Loftus, M.V. Romalis, B.R. Heckel, E.N. Fortson, Phys. Rev. Lett. **102**, 101601 (2009)
66. M. Dugan, B. Grinstein, L.J. Hall, Nucl. Phys. B **255**, 413 (1985)
67. S. Dimopoulos, S.D. Thomas, Nucl. Phys. B **465**, 23 (1996). arXiv:hep-ph/9510220
68. J. Hisano, M. Nagai, P. Paradisi, Phys. Rev. D **80**, 095014 (2009). arXiv:0812.4283 [hep-ph]
69. F.J. Botella, M. Nebot, O. Vives, J. High Energy Phys. **0601**, 106 (2006)
70. J.R. Ellis, R.A. Flores, Phys. Lett. B **377**, 83 (1996). arXiv:hep-ph/9602211
71. A. Manohar, H. Georgi, Nucl. Phys. B **234**, 189 (1984)
72. M. Ahmed et al. (MEGA Collaboration), Phys. Rev. D **65**, 112002 (2002). arXiv:hep-ex/0111030
73. L. Calibbi, A. Faccia, A. Masiero, S.K. Vempati, J. High Energy Phys. **0707**, 012 (2007). arXiv:hep-ph/0610241
74. R.M. Carey et al. (Mu2e Collaboration), FERMILAB-PROPOSAL-0973
75. Y.G. Cui et al. (COMET Collaboration), KEK Report 2009-10
76. A.G. Akeroyd et al. (SuperKEKB Physics Working Group), arXiv:hep-ex/0406071
77. M. Bona et al., arXiv:0709.0451 [hep-ex]
78. A.J. Buras, L. Calibbi, P. Paradisi, J. High Energy Phys. **1006**, 042 (2010). arXiv:0912.1309 [hep-ph]
79. A. Abada, A.J.R. Figueiredo, J.C. Romao, A.M. Teixeira, J. High Energy Phys. **1010**, 104 (2010). arXiv:1007.4833 [hep-ph]
80. A. Abada, A.J.R. Figueiredo, J.C. Romao, A.M. Teixeira, arXiv:1104.3962 [hep-ph]
81. B.C. Allanach, J.P. Conlon, C.G. Lester, Phys. Rev. D **77**, 076006 (2008). arXiv:0801.3666 [hep-ph]
82. G. Isidori, Y. Nir, G. Perez, arXiv:1002.0900 [hep-ph]
83. A.J. Buras, D. Guadagnoli, Phys. Rev. D **78**, 033005 (2008). arXiv:0805.3887 [hep-ph]
84. E. Barberio et al. (Heavy Flavor Averaging Group), arXiv:0808.1297 [hep-ex]
85. M. Bona et al. (UTfit Collaboration), PMC Phys. A **3**, 6 (2009). arXiv:0803.0659 [hep-ph]
86. V.M. Abazov et al. (D0 Collaboration), Phys. Rev. D **82**, 032001 (2010). arXiv:1005.2757 [hep-ex]
87. V.M. Abazov et al. (D0 Collaboration), arXiv:1106.6308 [hep-ex]
88. R. Barbieri, G. Isidori, J. Jones-Perez, P. Lodone, D.M. Straub, arXiv:1105.2296 [hep-ph]
89. C. Aubin, J. Laiho, R.S. Van de Water, Phys. Rev. D **81**, 014507 (2010). arXiv:0905.3947 [hep-lat]
90. J. Charles et al. (CKMfitter Group Collaboration), Eur. Phys. J. C **41**, 1–131 (2005). arXiv:hep-ph/0406184, http://ckmfitter.in2p3.fr
91. J. Laiho, E. Lunghi, R.S. Van de Water, Phys. Rev. D **81**, 034503 (2010). arXiv:0910.2928 [hep-ph]
92. A.J. Buras, M. Jamin, P.H. Weisz, Nucl. Phys. B **347**, 491–536 (1990)
93. J. Brod, M. Gorbahn, Phys. Rev. D **82**, 094026 (2010). arXiv:1007.0684 [hep-ph]
94. J. Brod, M. Gorbahn, arXiv:1108.2036 [hep-ph]
95. G. Buchalla, Phys. Lett. B **395**, 364–368 (1997). arXiv:hep-ph/9608232
96. A.J. Buras, D. Guadagnoli, G. Isidori, Phys. Lett. B **688**, 309–313 (2010). arXiv:1002.3612 [hep-ph]
97. V. Lubicz, C. Tarantino, Nuovo Cimento B **123**, 674–688 (2008). arXiv:0807.4605 [hep-lat]
98. Y. Grossman, Y. Nir, G. Perez, Phys. Rev. Lett. **103**, 071602 (2009). arXiv:0904.0305 [hep-ph]
99. C.W. Bauer, N.D. Dunn, Phys. Lett. B **696**, 362 (2011). arXiv:1006.1629 [hep-ph]
100. (LHCb Collaboration), LHCb-CONF-2011-056
101. A.J. Buras, D. Guadagnoli, Phys. Rev. D **79**, 053010 (2009). arXiv:0901.2056 [hep-ph]
102. A. Lenz et al., Phys. Rev. D **83**, 036004 (2011). arXiv:1008.1593 [hep-ph]
103. S.K. Lamoreaux, Phys. Rev. A **66**, 022109 (2002). arXiv:nucl-ex/0109014
104. HfF^+ eEDM Experiment, http://jilawww.colorado.edu/bec/index.html

105. PbO eEDM Experiment, http://www.yale.edu/demillegroup
106. YbF eEDM Experiment, http://www3.imperial.ac.uk/ccm/research/edm
107. CryoEDM Experiment, http://hepwww.rl.ac.uk/EDM/index_files/CryoEDM.htm
108. PNPI nEDM Experiment, http://nrd.pnpi.spb.ru/LabSereb/neutronedm.htm
109. PSI nEDM Experiment, http://nedm.web.psi.ch
110. SNS nEDM Experiment, http://p25ext.lanl.gov/edm/edm.html
111. J. Alwall, M. Herquet, F. Maltoni, O. Mattelaer, T. Stelzer, J. High Energy Phys. **1106**, 128 (2011). arXiv:1106.0522 [hep-ph]
112. T. Sjostrand, S. Mrenna, P.Z. Skands, J. High Energy Phys. **0605**, 026 (2006). arXiv:hep-ph/0603175
113. http://www.physics.ucdavis.edu/~conway/research/software/pgs/pgs.html